RECOGNITION OF PLATINUM-DNA ADDUCTS BY HMG-BOX PROTEINS

Srinivas Ramachandran

A dissertation submitted to the faculty of the University of North Carolina at Chapel Hill in partial fulfillment of the requirements for the degree of Doctor of Philosophy in the Department of Biochemistry and Biophysics

Chapel Hill
2011

Approved by:
Sharon L. Campbell
Stephen G. Chaney
Nikolay V. Dokholyan
Gerhard Meissner
Brian D. Strahl

ABSTRACT

Srinivas Ramachandran: Recognition of platinum-dna adducts by hmg-box proteins
(Under the direction of Nikolay V. Dokholyan)

Cisplatin (CP) and oxaliplatin (OX) are platinum (Pt) based drugs that are widely used in chemotherapy. The mode of action of Pt drugs is through the formation of Pt adducts on intrastrand guanines (5'GG) in genomic DNA. A class of proteins that bind specifically to Pt adducts contain the HMG-domain, which is found in both abundant housekeeping proteins like HMGB1 and also in low abundance transcription factors. The differential affinity of HMG-domain proteins to CP- and OX-DNA may play a role in the differential efficacies of CP- and OX-DNA. In this study, we aim to understand the molecular basis of the differential affinity of HMGB1a to CP- and OX-DNA, given that the only differences between these two species is their carrier ligand, which is not even involved in the Protein-DNA interface. We hypothesized that the differences in conformational dynamics rather than the major conformation of Pt-DNA determines the differential binding affinity to HMGB1a. To test this hypothesis, we performed molecular dynamics simulations of both free Pt-DNA and HMGB1a-Pt-DNA complexes. Our simulations of free Pt-DNA revealed that the conformational dynamics of CP- and OX-GG adducts are distinct and depend on the sequence context of the adduct. We found that the minor conformations sampled exclusively by the CP-GG adduct exhibit structural properties that favor binding by HMGB1a, while these conformations are not sampled by OX-GG adducts. Comparing the conformations of Pt-DNA in three sequence contexts revealed the sequence and carrier ligand dependent distortions induced by the Pt-GG adduct. Finally, simulations of HMGB1a-Pt-DNA revealed that the lack of flexibility of

OX-DNA in the TGGA sequence context seen in free Pt-DNA translated to a much weaker binding interface compared to CP-DNA, thus explaining the experimentally observed low binding affinity of OX-DNA compared to CP-DNA. Based on these results, we postulate that the carrier ligand affects the DNA conformations explored by Pt-GG adduct, which influences the binding affinities of HMG-domain proteins for Pt-GG adducts, and that these conformations are further influenced by the DNA sequence context of the Pt-GG adduct.

To thatha

ACKNOWLEDGEMENTS

The completion of this dissertation has relied on the belief and the judgment of a lot of people. I would like to thank Prof. Barry Lentz for making me a part of the wonderful biophysics program at UNC, which provided me the opportunity to meet my advisor Nikolay Dokholyan. The professional and scientific development of his students is of utmost importance to Nikolay, and I have benefitted a lot from this attitude. Through the efforts of Nikolay and every member of dokhlab, I could be a part of a tight-knit team that enjoyed doing science and was highly productive. Prof. Stephen Chaney and Prof. Gerhard Meissner could be described as two pillars of my doctoral work. Working closely with them over the years has given me rich insight and opportunity to work on platinum drugs and ryanodine receptors. I would like to thank Brenda Temple, whose advice, help and prior work made all the simulations possible. I have enjoyed collaborating with Brian Strahl, Xian Chen, and Sharon Campbell in various projects that have been exciting as well as fruitful. Finally, I am indebted to my family and friends for providing encouragement and entertainment at all times I was away from the lab.

PREFACE

Part of the work described in this dissertation was published as an article in Nucleic Acids Research:

Srinivas Ramachandran, Brenda R. Temple, Stephen G. Chaney and Nikolay V. Dokholyan, **Structural basis for the sequence-dependent effects of platinum-DNA adducts.** *Nucleic Acids Research* (2009) 37(8):2434-2448

Required permission to reuse figures and text extracts from the article has been obtained from all the authors and Oxford University Press (Journal Publisher).

Table of Contents

List of Tables

List of Figures

List of Abbreviations

CP	Cisplatin
HMGB1	High-mobility group protein 1
HMGB1a	Domain A of High-mobility group protein
HR	Homologous recombination
MMR	Mismatch repair
NER	Nucleotide excision repair
OX	Oxaliplatin
Pt	Platinum
TBP	Tata box binding protein

CHAPTER 1. Introduction

Platinum (Pt) based drugs are widely used chemotherapy agents. Even 40 years after the serendipitous discovery of the first Pt-drug, Pt-based chemotherapeutic regimens are still the treatment of choice for many solid tumors, and are increasingly being used in combination with newly developed targeted therapies (Wang and Lippard, 2005). Since the discovery of the first Pt drug, more than 3000 analogs with a Pt core have been developed (Weiss and Christian, 1993), but to date, only cisplatin (cis-Diamminedichloroplatinum(II), CP), carboplatin (cis-diammine-1,1-cyclobutane dicarboxylate) and oxaliplatin ((trans-R,R)1,2-Diaminocyclohexaneoxalatoplatinum(II) have been approved for clinical use in the US (Figure 1.1).

Unfortunately, treatment with CP is accompanied by serious side effects that include nephrotoxicity, neurotoxicity, ototoxicity, nausea and vomiting which are dose-limiting. Even though carboplatin has the same tumor range as CP, and in many cases is less effective, it is mainly used in treatment due to the reduced severity of the side effects in carboplatin treatment as compared to CP treatment. OX, which is approved for only colon cancer in the US, has side effects that include neuropathy, nausea, vomiting and diarrhea. Another major disadvantage of CP and carboplatin in cancer therapy is the innate and acquired resistance to CP and carboplatin exhibited by many tumors.

Pt drugs are widely used despite their serious side effects because of their effectiveness in inhibiting proliferation in a broad spectrum of cell types. CP and carboplatin are used in the treatment testicular, ovarian, head, neck and non-small cell

lung cancer. CP is especially effective in treating testicular cancer, with cure rates of 90% (Bosl, et al., 2008). OX is used in the treatment of colorectal and other cancers, where CP is not effective. Thus, the Pt drugs currently in use present a double edged sword: they are some of the most potent chemotherapeutic agents in use, but their severe side effects and acquired resistance severely limit their effectiveness. These disadvantages of currently approved Pt drugs have prompted exploration of several analogs. **However, understanding the biological mechanisms that are involved in Pt cytotoxicity and Pt resistance is essential to develop better chemotherapeutic agents.**

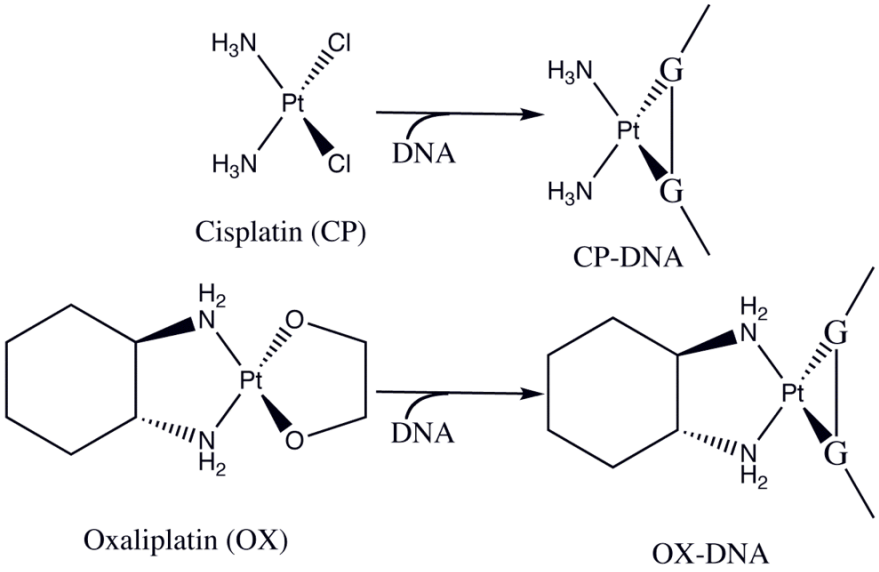

Figure 1.1. Platinum drugs and their GG intrastrand adducts on DNA

1.1. Mechanism of Cytotoxicity and Resistance

Pt drugs reduce proliferation of tumor cells by directly bringing about cancer cell death. In this regard, Pt drugs bring about death of any dividing cells by forming Pt-DNA adducts. Thus, the various processes that affect Pt drug effectiveness would include cellular uptake and efflux of the drug, transport of the drug to the nucleus, adduct formation on genomic DNA, recognition of Pt-DNA adducts by a host of DNA-binding

proteins including DNA damage response proteins and the subsequent activation of various cellular pathways that lead to apoptosis, necrosis, repair or mutagenesis (Jung and Lippard, 2007) (Figure 1.2). Pt drug sensitivity would be increased by effective uptake, minimal efflux, effective transport to nucleus, high density of adduct formation, and activation of downstream pathways that lead to apoptosis. It is important to note that not only increasing the rate of apoptosis, but also reducing efflux and repair rates would increase Pt drug effectiveness.

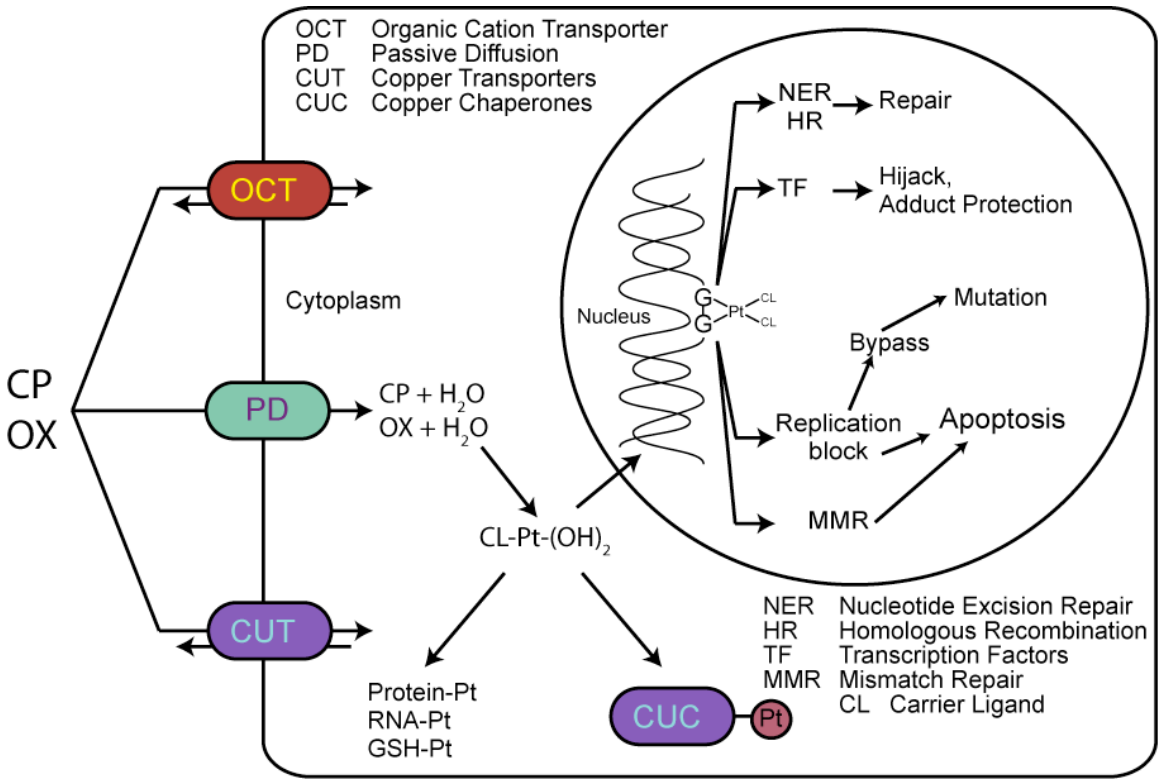

Figure 1.2. Transport and cellular fate of Pt drugs.
The most significant aspects of cisplatin (CP) and oxaliplatin (OX) cellular toxicities are illustrated.

The primary mode of cellular uptake of Pt drugs has been thought to be by passive diffusion since the drug uptake by cells is not saturable (Binks and Dobrota, 1990; Gale, et al., 1973; Hromas, et al., 1987) and uptake of a Pt drug is not inhibited by its analogs (Gately and Howell, 1993). Additionally, proteins involved in copper homeostasis (including copper transporters and chaperones) have been implicated in

drug uptake and efflux (Safaei and Howell, 2005). Organic Cation Transporters (especially OCT2) are thought to be responsible for nephrotoxicity of CP due to their selective expression in kidney, where they are the main mediators of Pt drug uptake (Ciarimboli, et al., 2005; Yonezawa, et al., 2006).

Upon cellular entry, the leaving groups (two chloride ligands in CP and oxalate ligand in OX) are replaced by two water ions, conferring a net positive charge on the drugs (Pinto and Lippard, 1985), which would be effective in reducing the rate of efflux by passive diffusion through the membrane. Aquated CP and OX can form adducts with protein, RNA, and thiol-containing molecules like glutathione (Jung and Lippard, 2007). However, the largest amount of Pt adducts are formed on DNA, which has also been shown to be the primary cause of the cytotoxic effects of Pt drugs (Jung and Lippard, 2007). Pt adducts on DNA are formed through the reaction of Pt with N7 atoms of guanine or adenine (Bancroft, et al., 1990). Consequently, monofunctional adducts on adenine and guanine, and bifunctional interstrand, intrastrand adducts with either adenine or guanine or both are possible. However, calculations have shown that only AG, GG, GNG intrastrand adducts and interstrand adducts are probable (Baik, et al., 2003). In cellular DNA, both CP and OX form the same type of adducts at the same sites: 60-65% intrastrand GG, 25-30% intrastrand AG, 5-10% intrastrand GNG and 1-3% interstrand GG diadducts (Eastman, 1987).

The recognition of Pt-DNA adducts by various cellular proteins trigger downstream pathways that lead to either apoptosis or necrosis or the repair of lesions (Jung and Lippard, 2007). Repair of lesions is the most effective form of Pt drug resistance as it returns the DNA to pre-drug state. The main modes of repair of Pt-DNA adducts involve the Nucleotide excision repair (NER) pathway, recombination repair pathway and mismatch repair (MMR) pathway (Chaney, et al., 2005). NER is the most

effective form of repair of Pt-DNA lesions in cells, with cell lines deficient in NER pathway showing increased sensitivity to Pt drugs (Furuta, et al., 2002). Furthermore, CP-resistant cell lines have been shown to have increased levels of NER pathway transcripts (Weaver, et al., 2005). NER is efficient in repairing 1,3-GNG and 1,2-GG intrastrand and interstrand Pt-DNA adducts (Zamble, et al., 1996). Effective MMR is thought to be very important in CP sensitivity as opposed to NER, which may contribute to CP resistance (Chaney, et al., 2005). MMR pathway proteins actively seek to repair mismatches on newly synthesized DNA across Pt adducts, which if repeatedly unsuccessful would trigger ATR checkpoint (Jiricny, 2006). MMR also mediates DNA damage induced apoptosis (Bellacosa, 2001). MMR's role in CP sensitivity is highlighted by the fact that many CP-resistant cell lines feature defects in the MMR pathway (Vaisman, et al., 1998).

Pt-DNA adducts also block DNA- and RNA-polymerases during the process of replication and transcription respectively (Chaney, et al., 2005). Blockage of DNA-polymerases α, ε and γ results in the recruitment of error-prone bypass polymerases that attempt to replicate past the Pt adducts (Bassett, et al., 2003; Havener, et al., 2003; Vaisman, et al., 2000). Failure to bypass Pt adducts leads to cell cycle arrest (Siddik, 2003), while error-prone bypass results in mutations at the adduct site in daughter cells (Chaney, et al., 2005). These mutations are thought to lead to the development of secondary tumors or Pt drug resistance (Chaney, et al., 2005). Block of RNA-polymerase by Pt-DNA adducts on the other hand results in multiple outcomes. RNA pol II blocked by CP-DNA adducts has been shown to be mono- and poly-ubiquitinated, which may or may not lead to its degradation (Jung and Lippard, 2007). Blocked RNA pol II also triggers NER (through transcription coupled repair) and has been shown to mediate pathways that lead to programmed cell death (Svejstrup, 2003).

1.2. Interaction of Pt-DNA adducts with proteins

One of the major determinants of the eventual fate of cells exposed to Pt drugs is the recognition of Pt-DNA adducts by proteins that specifically interact with Pt-DNA or encounter Pt-DNA during the course of their function (polymerases for example). Some of the proteins shown to bind specifically to Pt-DNA adducts include XPC, XPA, RPA (part of NER pathway), hMSH2, hMutSalpha (part of MMR pathway), Ku80, P53, PARP-1, YB-1 (DNA damage response proteins) and TBP (transcription factor) (Chaney, et al., 2005). However, the highest specificity for binding Pt-DNA has been exhibited by HMG-domain proteins. Several HMG domain proteins such as HMG1 (Pil and Lippard, 1992), HMG2 (Lawrence, et al., 1993), Ixr1 (Brown, et al., 1993; McA'Nulty and Lippard, 1996), tsHMG (Ohndorf, et al., 1997), SRY (Chow, et al., 1994), SSRP1 (Yarnell, et al., 2001), LEF-1 (Chow, et al., 1994; Chvalova, et al., 2008) and hUBF (Treiber, et al., 1994; Zhai, et al., 1998) bind with high affinity to Pt adducts. Proteins with HMG-domain that bind to Pt-GG adducts fall into two classes: structure-specific, abundant, chromatin architectural proteins like HMGB1 and sequence-specific, cell-type specific transcription factors like LEF-1 and SRY. The binding of structure-specific HMG-domain proteins to Pt-DNA adducts has been shown to inhibit nucleotide excision repair (Huang, et al., 1994; McAnulty and Lippard, 1996), which may increase the longevity of Pt-DNA adducts. Pt-DNA adducts have also been postulated to sequester some HMG-domain containing transcription factors that are essential for maintaining the uncontrolled cell growth characteristic of tumor cells (Treiber, et al., 1994; Zhai, et al., 1998). Thus, the binding of HMG-domain proteins to Pt-DNA could significantly sensitize cells to CP and OX.

A crystal structure of HMGB1a in complex with CP-GG DNA in the TGGA sequence context (Ohndorf, et al., 1999) has been reported (Figure 1.3). That structure, coupled with site-directed mutagenesis, has provided considerable insight into the

mechanism of HMGB1a binding to Pt-DNA adducts, which can be extrapolated to understand binding of other HMG-domain proteins to Pt-DNA adducts. There are a number of hydrophobic and hydrogen bond interactions between HMGB1a and the minor groove of DNA on the 3' side of the CP-GG adduct. Among these interactions, the most significant appears to be the intercalation of Phe37 between the two Gs of the Pt-GG adduct, which allows a π-π stacking interaction between Phe37 and the 3' G (Figure 1.3B). Mutation of Phe37 to Ala resulted in more than 667-fold decrease in binding affinity (He, et al., 2000). Thus, Phe37 in HMGB1a specifically recognizes the distortion caused by formation of the Pt-GG adduct. Several other structures of HMG-domain proteins bound to undamaged DNA reveal similar intercalation, but involving different residues (methionine, in LEF-1 (Love, et al., 1995) and isoleucine in SRY (Werner, et al., 1995)for example).

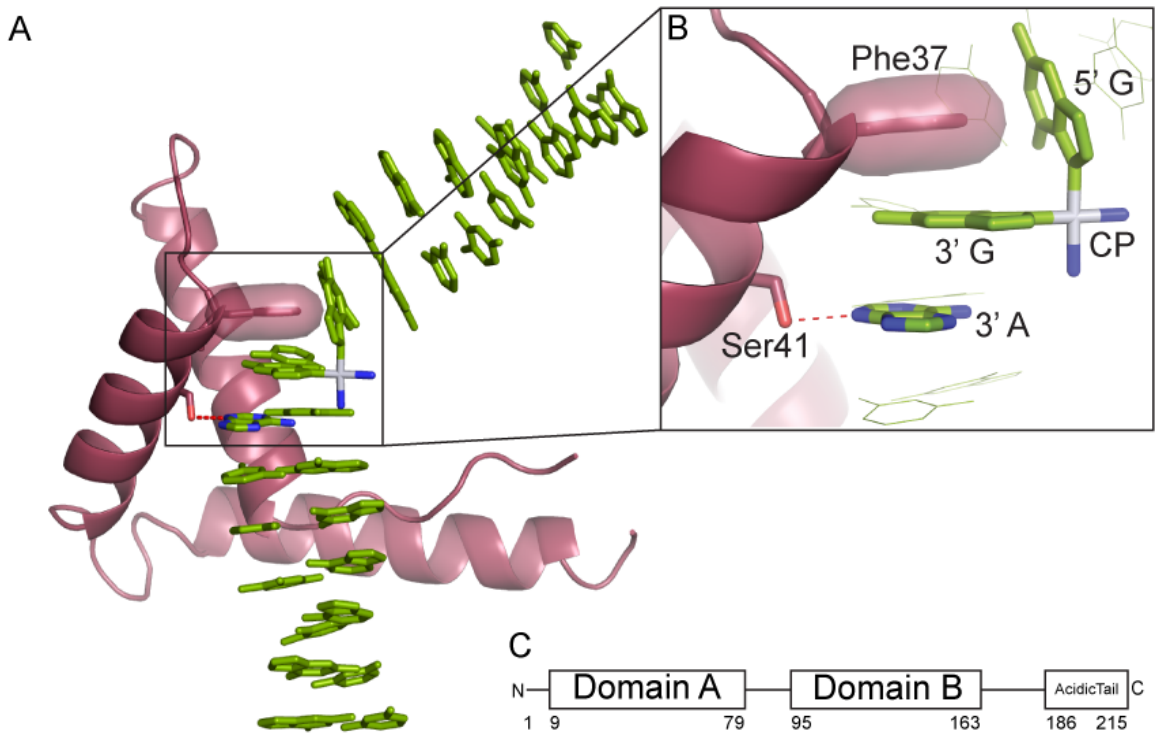

Figure 1.3 The Pt-DNA-HMGB1a Complex
A) The crystal structure of HMGB1a bound to CP-DNA (PDB ID 1CKT) B) A zoomed in view showing the important interactions C) The Domain structure of HMGB1

The crystal structure of HMGB1a bound to Pt-DNA in the TGGA sequence context (Ohndorf, et al., 1999) also shows a hydrogen bond between Ser41 and the N3 atom of Adenine 3' of the Pt-GG adduct (Figure 1.3B). A Ser41Ala mutation resulted only in a 3.9-fold decrease in binding affinity, a much weaker effect than the Phe37Ala mutation (He, et al., 2000). This interaction would depend on the conformation of the base-pair on the 3' side of the adduct, which may be influenced by the sequence context of the adduct. The contributions of other interactions between HMGB1a and the minor groove of Pt-DNA adducts to the binding affinity of the protein-DNA complex have not been characterized, but are likely to be less than or equal to the Ser41-3'A-N3 interaction.

1.3. Proposed mechanisms of cellular discrimination between CP and OX

One of the phenomena that add to the complexity of cellular toxicity due to Pt drugs is the difference in tumor range of CP and OX. Even though CP and OX form similar adducts at similar sites on DNA, cells and tumors that are resistant to CP are generally not cross resistant to OX (Chaney and Vaisman, 1999; Rixe, et al., 1996). The lack of cross-resistance of cells to CP and OX is thought to be in part due to the effects downstream of formation of CP- and OX-DNA adducts (Chaney, et al., 2005). **Since the only difference between CP and OX is their carrier ligand, the differences in cytotoxicity indicate the importance of carrier ligand in the overall effect of a Pt drug. Thus, understanding the molecular basis of differences in cytotoxicity between CP and OX will provide information for better design of Pt drug analogs.**

Strikingly, many of the elements of Pt-DNA response discussed in 1.2 do not influence the difference in sensitivity of tumors to CP and OX. NER and recombination repair have been shown to not distinguish between CP- and OX-DNA adducts (Reardon,

et al., 1999; Wu, et al., 2004). In contrast to NER status, MMR proficiency selectively sensitizes cells to CP, but even mismatch repair proficient colon cancer cells are more sensitive to OX than to CP (Vaisman, et al., 1998). Moreover, the effect of MMR on the cytotoxicity of CP-DNA adducts is 2-fold or less (Aebi, et al., 1996; Drummond, et al., 1996; Fink, et al., 1996), while differences in the cytotoxicity of CP- and OX-DNA adducts are often 5-10-fold (Page, et al., 1990; Schmidt and Chaney, 1993). Replicative DNA polymerases and most translesion polymerases are blocked by OX-DNA and CP-DNA adducts with equal efficiency (Chaney and Vaisman, 1999; Havener, et al., 2003). Pol η is somewhat better at bypassing OX-DNA adducts than CP-DNA adducts (Vaisman, et al., 2000), but the outcome of this difference is manifested as differences in mutagenicity rather than cell survival (Bassett, et al., 2004). Taken together these observations indicate that important cellular activities other than DNA repair proficiency influence cellular sensitivity to different platinum drugs.

In contrast to the lack of discrimination between CP- and OX- by different repair recognition proteins, HMG-domain proteins like HMGB1, LEF-1, TBP and hUBF are known to bind CP- and OX adducts with different affinities (Chvalova, et al., 2008; Malina, et al., 2007; Wei, et al., 2001). Consequently, the differential binding affinities of HMG domain proteins to CP- and OX-DNA adducts have been proposed to contribute to the distinctive cellular effects of CP- and OX-DNA adducts. For example, HMGB1 has also been shown to inhibit translesion synthesis past CP-adducts to a greater extent compared to OX-adducts (Vaisman, et al., 1999) and will similarly be expected to shield CP-adducts from NER better than OX-adducts. Furthermore, HMGB1 expression is elevated in many cancer types, including colorectal cancers (Volp, et al., 2006), which frequently display resistance to CP but not OX (Raymond, et al., 1998; Rixe, et al., 1996). Hence, understanding the basis of the differential binding of HMG domain

proteins to CP- and OX-DNA could lead to a better understanding of the differential efficacies of CP and OX.

The binding of HMGB1 to Pt-DNA adducts has been characterized in great detail. HMGB1 contains two HMG domains: domain A (HMGB1a) and domain B (HMGB1b) (Figure 1.3C). HMGB1a binds more strongly than HMGB1b to most Pt-GG DNA adducts (Wei, et al., 2001). Full length HMGB1 binds with lower affinity compared to HMGB1a mainly due to its highly acidic C-terminal tail (Figure 1.3C), which when removed results in the tandem HMG domains having same affinity as HMGB1a (Jung and Lippard, 2003). However, HMGB1a binds to Pt-GG adducts with the same specificity as full length HMGB1 (Jung and Lippard, 2003). Further, footprinting studies combined with site-directed mutagenesis have shown that only domain A of full length HMGB1 binds to DNA containing the Pt-GG DNA adduct (He, et al., 2000; Jung and Lippard, 2003). Thus, most of the structural and mechanistic studies have been performed with HMGB1a alone. The differential binding affinity of HMGB1a towards CP- and OX-DNA is also dependent on the identity of bases flanking the central intrastrand GG (Malina, et al., 2007; Wei, et al., 2001). The binding affinity of HMGB1a for CP-DNA adducts has been shown to be ~53 times greater than that for OX-DNA adducts in the TGGA sequence context (Wei, et al., 2001) while in the AGGC (Wei, et al., 2001) and the CGGA (Malina, et al., 2007) sequence contexts, the binding affinity for CP-DNA is only 3 times greater than that of OX-DNA adducts. In the TGGT sequence contest, the binding affinity of HMGB1a for CP-GG and OX-GG adducts is almost the same (Malina, et al., 2007). Most of the sequence-dependent variations in differential binding affinity of HMGB1a towards CP- and OX-DNA adducts is due to sequence dependent effects for binding to OX-DNA adducts since the binding affinity of HMGB1a for CP-GG adducts is roughly comparable in all three sequence contexts (Malina, et al., 2007; Wei, et al., 2001). This sequence

dependent effect has also been shown for HMGB1b and TBP, but the trends are slightly different (Wei, et al., 2001).

1.4. Distortion of DNA structure by Pt-adduct formation

Since the differential cellular effects of CP and OX seem to stem from differential binding of proteins to CP- and OX-DNA adducts, we could expect significant differences in the structures of CP- and OX-DNA adducts, leading to differential recognition. To examine the effect of Pt-adducts on DNA structure, oligomers made up of 8-12 base-pairs, containing single Pt-adducts have been characterized in great detail by Xray crystallography and NMR spectroscopy (Gelasco and Lippard, 1998; Herman, et al., 1990; Marzilli, et al., 2001; Spingler, et al., 2001; Takahara, et al., 1996; Wu, et al., 2007; Wu, et al., 2004; Yang, et al., 1995). Even though various types of adducts like monofunctional, interstrand and GNG intrastrand adducts have been characterized, the structural characteristics of the most abundant adducts; the 1,2 GG intrastrand adducts are of importance, especially because HMG-domain proteins selectively bind these adducts. Pt-GG adducts are formed on the major groove of DNA, where the N7 atoms of the guanines are exposed. The geometry of the Pt ligands induces a large roll in the platinated GG base-pair step. The increased roll directly leads to the pronounced bending of DNA towards the major groove. The helix is also locally unwinded at the site of the adduct and the minor groove is shallow and wide.

Comparing the structures of CP- and OX-DNA adducts in the same sequence context (T<u>GG</u>T) by X-ray crystallography revealed almost identical structures. In the A<u>GG</u>C sequence context, where binding of HMGB1a to CP- and OX-DNA differs by 3 fold, only minor differences were detected in structural characterization by NMR. In the TGGA sequence context, where the differences in binding energy is almost 53-fold, MD simulations indicate minimal differences in the overall conformations of CP- and OX-

DNA. Thus, structural studies indicate no major structural differences in average conformations between CP- and OX-DNA in three different sequence contexts. Furthermore, the carrier ligand cannot influence binding affinity by direct interactions with the protein since the HMG-domain proteins and TBP bind to the major groove of DNA, while the adduct is formed on the major groove.

1.5. Motivation

The structural data for CP- and OX-DNA adducts suggest that the average conformation of CP- and OX-DNA adducts are similar. Further, since the HMG-domain proteins and TBP bind DNA through the minor groove, the carrier ligand could influence binding only indirectly. Even though the average structures of CP- and OX-DNA are similar, the conformational dynamics of DNA may lead to some minor conformations of CP- and OX-DNA to be distinct from each other. These minor conformations may facilitate increased binding to HMG-domain proteins, thus influencing the differential binding affinities observed. Thus, we have hypothesized that differences in the conformational dynamics of CP and OX adducts may give rise to the differences in their activity.

In this study, we use molecular dynamics simulations, which can probe short time-scale conformational dynamics, to examine the effect of carrier ligand on the conformational space of free Pt-DNA. We then perform simulations of HMGB1a-Pt-DNA complex to explore the differences in the binding interfaces of HMGB1a with CP- and OX-DNA that lead to their differential binding affinities. These simulations provide the molecular basis of differences in binding of HMGB1a to CP- and OX-DNA and also illustrate the effect of carrier ligand on the conformational dynamics and flexibility of Pt-DNA.

Chapter 2. Materials and Methods

2.1. DNA and protein constructs used in the simulations

Pt-DNA Simulations. We performed simulations on a 12-mer DNA sequence (shown in Scheme 1), which was either undamaged or covalently bound to CP or OX at the N7 of G6 and G7. We used the solution structure of OX-TGGT adduct determined by NMR spectroscopy as the starting structure for the OX-TGGT simulations. In the same structure, the adduct was modified to cisplatin for the CP-TGGT simulations. The initial structures for the CP- and OX-TGGA simulations were obtained by modifying the NMR structure of OX-DNA in the TGGT sequence context. We chose this structure because of the NMR solution structures of Pt-DNA adducts that we have obtained it was closest in sequence to the TGGA sequence context. Using INSIGHT II (Accelrys Inc., CA), the T8-A17 base pair was replaced by the A8-T17 base pair in the TGGT NMR structure to obtain the initial structure of OX-DNA in TGGA sequence context. Further, OX was modified to CP to obtain CP-DNA structure in the TGGA sequence context. INSIGHT II was used to generate canonical B-DNA structure, which was used as the starting structure for simulations of the undamaged DNA. Data for the AGGC sequence context were obtained from simulations that were performed as part of an earlier work (Sharma, et al., 2007).

HMGB1a-Pt-DNA Simulations. For the simulations of HMGB1a-Pt-DNA complex, we used the crystal structure of rat HMGB1a bound to CP-DNA in the TGGA sequence context as the starting structure for the CP-TGGA simulations (PDB ID 1CKT

(Ohndorf, et al., 1999)). This structure was modified appropriately using Insight II to generate starting structures for OX-TGGA, CP-AGGC and OX-AGGC simulations.

Scheme 1. Dodecamer sequences used in simulations.

```
                                5678
TGGA sequence context: 5′-d(CCTCTGGACTCC)-3′
                       3′-d(GGAGACCTGAGG)-5′
                                5678
AGGC sequence context: 5′-d(CCTCAGGCCTCC)-3′
                       3′-d(GGAGTCCGGAGG)-5′
                                5678
TGGT sequence context: 5′-d(CCTCTGGTCTCC)-3′
                       3′-d(GGAGACCAGAGG)-5′
```

2.2. Force Field.

The force field parameters used for DNA and protein were from the Duan et al. force field (Cornell, et al., 1995; Duan, et al., 2003) with the ff03 parameter set. The partial charges for the Pt-GG adducts were derived by Sharma *et al.* (Sharma, et al., 2007). In order to determine the atomic partial charges of CP-GG and OX-GG adducts, the 9-methyl-guanine derivatives cis- [Pt(NH3)2(9-Me-Guo)2]2+ (CP-meG2) and [Pt(trans-RR-1,2-diaminocyclohexane)(9-Me-Guo)2]2+ (OX-meG2) were used. These derivatives were built from our NMR solution structures using Insight II. The atomic partial charges were determined using the Mulliken method implemented within Gaussian03 based on the NMR structure modified to the 9-methyl-guanine derivative. The density functional method B3LYP implemented within Gaussian03 was utilized; the LanL2DZ basis set was used for the platinum atom and 6-31Gd basis set was used for the rest of the atoms. Besides the atomic partial charges, other force field parameters of the Pt-GG adducts were referenced from AMBER parm99 force field parameters or from previous work by Yao et al (Yao, et al., 1994). and Scheeff et al (Scheeff, et al., 1999).

2.3. MD Simulations

Pt-DNA Simulations. We performed five sets of simulations of CP-, OX- and undamaged DNA in the TGGT and TGGA sequence contexts. Similar starting structures but randomized initial velocities were used in each of the five sets of simulations. The starting structures described above were first modified by removal of hydrogen atoms in Insight II. The structures were then prepared by LEaP module of AMBER v8.0 as follows: First hydrogen atoms were added back according to the nucleotide templates in AMBER force field library. Secondly the structures were neutralized with Na^+ ions. Thirdly the neutralized system was fully solvated in an octahedral water box using TIP3 model water molecules. The distance between the wall of the periodic box and the closest atom in the solute was set to be 12.5 Å. The Duan et al. force field (Cornell, et al., 1995; Duan, et al., 2003) with the ff03 parameter set was used, as well as our self-defined force field parameters for Pt-GG adducts.

Simulation Parameters. The non-bonded cutoff was set to be 9.0 Å and the non-bonded list was updated every 10 steps. The MD simulations were always carried out in NPT condition (constant pressure, using isotropic position scaling, at 1 atm (1 atm = 6.9 kPa), pressure relaxation time constant 0.2 ps in relaxation MD and 2 ps in production MD; constant temperature, using weak-coupling algorithm, at 300 K, heat bath coupling time constant 0.2 ps in relaxation MD and 1 ps in production MD) with a 1 fs time step. The SHAKE algorithm was applied to all bonds involving hydrogen atoms and in turn the regular force evaluation omitted for those bonds. The translational center-of-mass motion was removed every 1 ps. Every time when the system was heated, zero velocity information was inherited from the previous stage and a Maxwell distribution of velocities was re-established. In minimization and relaxation, a harmonic potential was applied to Pt-DNA adduct or DNA to restrain its motion. The restraint was gradually

weakened and became zero at the final stage of relaxation. The following 10 ns production MD was carried out unrestrained.

Simulation Protocol. The whole system underwent 120 ps minimization and relaxation before a 10 ns production MD carried out by the SANDER module of AMBER v8.0. The details of system minimization and relaxation were as follows. First, the whole system, including Pt-DNA adducts or undamaged DNA, water molecules and counter-ions, was minimized for 2000 steps using the steepest descent method in constant volume condition with a harmonic potential of 500 kcal/mol $Å^2$ (1 cal = 4.184 J) applied to Pt-DNA or DNA to fix its conformation. Second, the system was heated from 0 K to 300 K and kept in NVT (constant volume and constant temperature) condition with the harmonic restraints unchanged in a 20 ps relaxation MD. Third, the system was further relaxed in another short 20 ps MD in NPT condition with the same harmonic constraints. Fourth, the system was further minimized for 2000 steps of steepest descent in constant volume condition three times, with a weakening harmonic potential of 500, 50 and 5 kcal/mol $Å^2$ respectively. Fifth, the system was heated from 10 K to 300 K and kept in NVT condition with the harmonic restraints of 5 kcal/mol $Å^2$ in a 20 ps relaxation MD. Sixthly, four rounds of 20 ps relaxation MD were carried out in NPT condition with a further weakening harmonic potential of 5, 1, 0.1 and 0 kcal/mol $Å^2$ respectively. Seventhly, the system was heated up from 10 K to 300 K in NVT condition with zero restraints in a 20 ps relaxation MD. Finally, the system was heated for the very last time from 100 K to 300 K at the beginning of 10 ns production MD.

HMGB1a-Pt-DNA Simulations. We performed three sets of 50 ns simulations for CP-, OX- and undamaged DNA bound to HMGB1a in the TGGA, AGGC and TGGT sequence contexts. The starting structures were similar for each of the three simulations, but the initial velocities were randomized. The starting structures described above were

prepared in a manner identical to that of free Pt-DNA, except that LEaP v.9.0 was used and the crystallographic waters were retained while building the system. The MD simulation parameters were identical to the free Pt-DNA simulations.

Simulation Protocol. The whole system underwent 140 ps minimization and relaxation before a 50 ns production MD carried out by the PMEMD module of AMBER v9.0. First, the whole system, including Pt-DNA adduct, protein, water molecules and counter-ions, was minimized for 5000 steps using the steepest descent method in constant volume condition. Second, the system was heated from 0 K to 300 K and in NVT (constant volume and constant temperature) conditions in a 20 ps relaxation MD. Third, the system was further relaxed in 100 ps MD in NPT. Finally, the system was heated from 200 K to 300 K in NVT condition for a 20 ps run before beginning the 50 ns production MD.

2.4. Analysis Protocols

Hydrogen bonds. All the trajectories were analyzed for the presence of hydrogen bonds between all possible donors and acceptors based on a distance cut-off of 3.5 Å between the donor and acceptor and an angular cut-off of 135º between donor-H-acceptor. In the free Pt-DNA simulations, in addition to the Watson-Crick interactions, hydrogen bonds were formed for a significant amount of time between Pt-amines and the surrounding base pairs. All the frames of the trajectory were classified based on the type of hydrogen bonds formed between Pt-amines and the adjacent bases.

Centroid structures. We calculated the average structures for both the complete ensembles of CP-, OX- and undamaged DNA and also for the ensembles forming different hydrogen bonds. Since average structures are not actual structures from simulations and may feature some abnormal bond lengths/angles, we assigned the

structure from each ensemble that had the lowest mass-weighted root-mean-square deviation (RMSD) to the average structure as the centroid structure of that ensemble (Sharma, et al., 2007).

Comparisons of structures using root mean square deviation (RMSD). We used RMSD to compare centroid structures from different ensembles. In these comparisons, we used only the atoms from the DNA part of the molecule in calculating the RMSD.

Helical parameters. Helical parameters were calculated for each snapshot of the trajectory using the CURVES program, version 5.3 (Lavery and Sklenar, 1996). The following CURVES parameters were extracted: global inter base-pair parameters: shift, slide, rise, tilt, roll and twist; global base-base parameters: shear, stretch, stagger, buckle, propeller and opening. Histograms were then constructed for each of these parameters as frequency of occurrence versus discrete units of each DNA helical parameter. The discrete units (bin width) were set as 0.2 Å for all the distance parameters and 2º for all the angular parameters. Histograms were plotted for parameters corresponding to the central 4 base pairs of the DNA oligomer (the adduct is formed on central 2 base pairs). These distributions were also clustered on the basis of the pattern of hydrogen bond formation between the DNA and the drug.

To calculate the *P*-value of the difference between helical parameters corresponding to CP-, OX-DNA and undamaged DNA and also between different hydrogen bonded species in CP- and OX-DNA, we used the Kolmogorov-Smirnov (KS) test (Press, et al., 1992). The lower cut-off threshold of significant differences was calculated by dividing each data set into 5 equal subsets and performing KS test comparing all possible combinations of the 5 subsets of divided data. The highest –

log(*P*) among the subsets of each data set was set as the threshold for that data set. When two data sets were compared, the difference between them was significant only if –log(*P*) of the comparison of the data sets was higher than the threshold. The ratio of –log(*P*) of the comparison of the data sets to their thresholds was calculated and then this ratio for all the parameters are represented as colors in a diagram (heat map). The ratios transition from white (lowest ratios) to blue then red (highest ratios) in the heat map. The range of KS ratios and their corresponding color are shown as a scale in the bottom of the heat maps.

Bend angle. Overall bend angles of the snapshots from the simulations were calculated using the program MADBEND (Strahs and Sclick, 2000). MADBEND uses the local tilt and roll parameters from the CURVES (version 5.3) output to calculate the overall bend angle. The bend angle was calculated for the central 10 base pairs of the oligomer centered at G6-G7 where the Pt-adduct is formed. The normalized histograms were plotted for bend angle versus percent occupancy with a bin width of 2º. The bend angle values were also clustered on the basis of the type of hydrogen bond formed.

Analysis of the Protein-DNA Interface. In the HMGB1a-Pt-DNA simulations, the protein-DNA interface was primarily characterized by determining Protein-DNA interface contacts. We define an interface contact as a heavy atom from protein and a heavy atom from DNA within 5 Å of each other. Using this definition, we determine the total number of interface contacts in a given snapshot and build histograms of this measure across simulations. We also determine the contact map for a given ensemble. A contact map is a matrix, where the each row is a nucleotide and each column is a protein residue. The elements of the matrix are the total number of contacts between each nucleotide (row) and each residue (column). These contact maps are represented as colors in a diagram (heat map). The values transition from white (lowest number of

contacts) to blue then red (highest number of contacts) in the heat map. The range of the number of contacts and their corresponding color are shown as a scale in the bottom of the heat maps. Contact maps from two different ensembles are further compared by subtracting one from another, generating a difference-contact map, which is also represented as a heat map. Another measure used in analyzing the protein-DNA interface is the fraction of native contacts. The fraction of native contacts is the ratio of the number of native contacts formed in a given structure to the total number of native contacts. We obtained the list of native contacts from the HMGB1a-CP-DNA crystal structure determined in the TGGA sequence context.

Chapter 3. Simulations of CP- and OX-DNA in the TGGA sequence context

A number of cellular proteins containing the HMG-domain have differential binding affinities to CP- and OX-DNA adducts (Chvalova, et al., 2008; Wei, et al., 2001; Zhai, et al., 1998), which might be important in determining the differential downstream effects of formation of CP- and OX-DNA adducts. Understanding the molecular basis of this differential binding is essential to uncover the effect of carrier ligand in protein binding. The lack of major differences between experimental structures of CP- and OX-DNA suggests that the major conformations of CP- and OX-DNA in a given sequence context are similar and are not the major drivers of the differential affinities to proteins. Thus, either minor conformations and/or difference in flexibility between CP- and OX-DNA should drive the differential binding affinities. Hence, we postulated that the differences in conformational dynamics of CP- and OX-DNA adducts might be responsible for the differential recognition of these adducts by HMG-domain proteins. To test this hypothesis, we performed all-atom molecular dynamics simulations on undamaged 12-mer DNA and CP- and OX-GG 12-mer DNA adducts in the TGGA sequence context in which the discrimination of HMGB1a between CP- and OX-GG adducts is 53-fold. The simulations attained equilibrium within the first few nanoseconds, with the all-atom mass weighted RMSD of OX- and undamaged DNA remaining less than 3 Å and that of CP-DNA remaining less than 4 Å throughout the simulation (Figure 3.1).

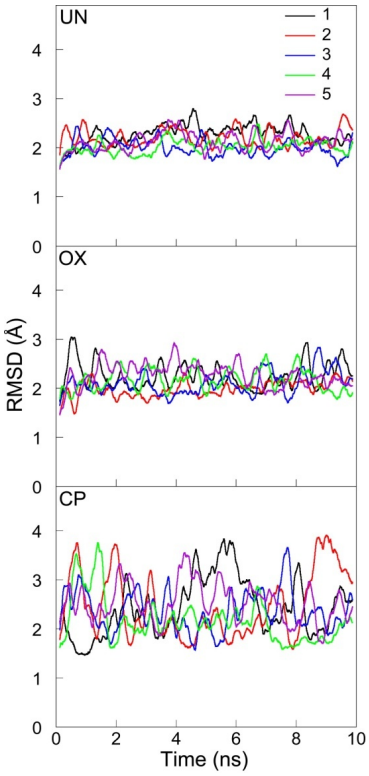

Figure 3.1. Average RMSD values for the MD simulations over time.
The RMSD values for each of the 5 simulations compared to the corresponding starting structure for the undamaged DNA, CP-DNA and OX-DNA are shown for the full 10 ns of each simulation. RMSD at time t represents the average of RMSD in a 250 ps bin centered at t (running average). The five simulation trajectories starting from undamaged DNA, CP-DNA and OX-DNA structures with different initial MD velocities are represented in black, red, blue, green and violet.

3. 1. The overall conformation of CP- and OX-GG adducts are similar

We first compared the centroid structures of CP- and OX-DNA simulations in the TGGA and the AGGC sequence contexts (Figure 3.2). The all-atom RMSD was ~2 Å when we compared either CP-TGGA with CP-AGGC or OX-TGGA with OX-AGGC, indicating lack of global structural differences in the major conformations sampled by CP- and OX-DNA adducts in the two sequence contexts. Even when we compared the centroid structures of CP- and OX-DNA in the TGGA sequence context (Figure 3.3C, RMSD=1.98 Å), there were no large conformational differences. The same comparisons for the central four base pairs of the centroid structures (Figure 3.2, D-F) yielded the same conclusion: the centroid structures did not display any major structural differences that would warrant high differential binding affinities between CP- and OX-DNA adducts.

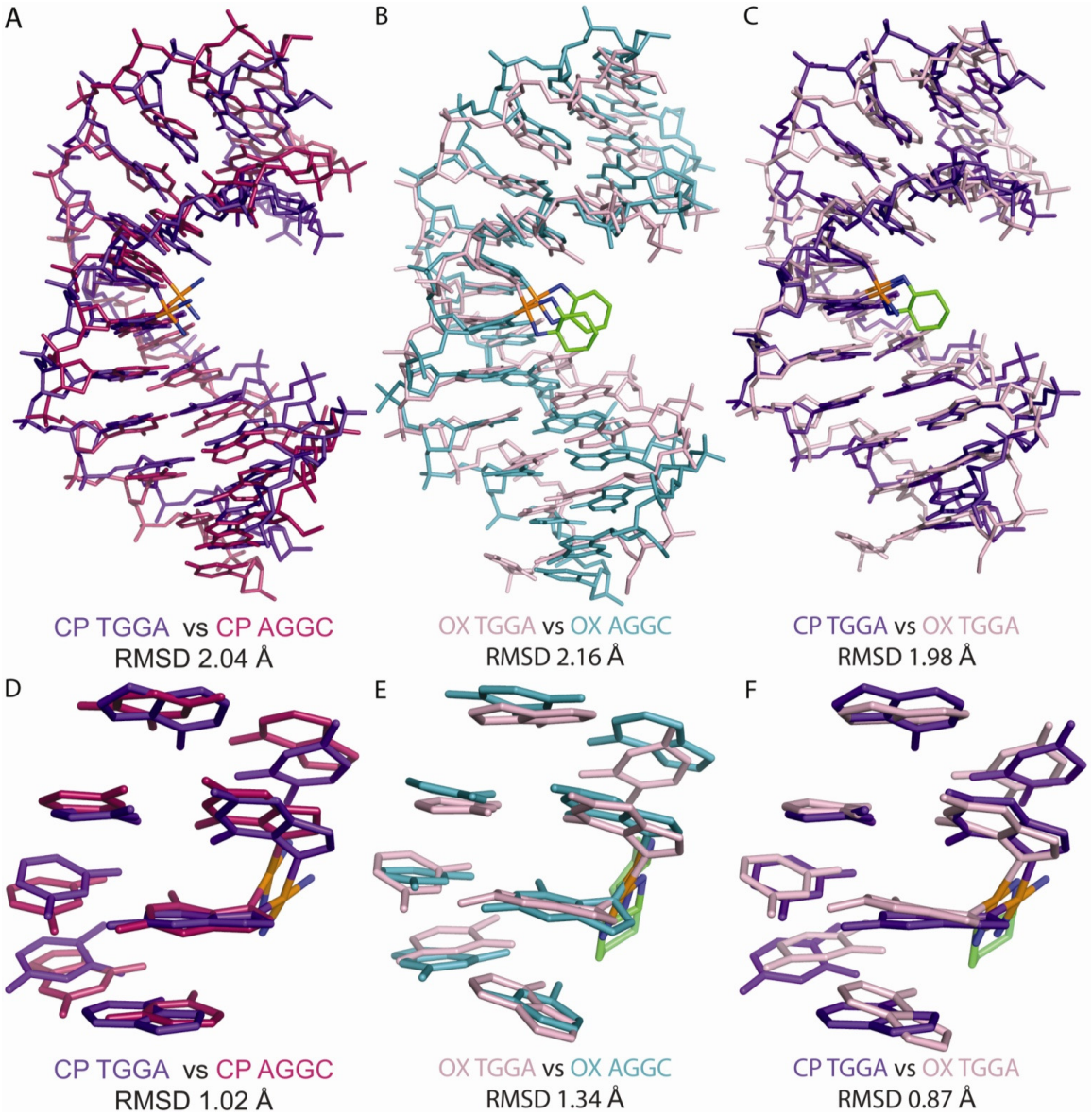

Figure 3.2. Comparison of centroid structures.
Structural alignment of the centroid structures using only the atoms from the DNA part of the molecule from the simulations of CP-DNA in AGGC and TGGA sequence contexts (**A**), OX-DNA in AGGC and TGGA sequence context (**B**) and CP- and OX-DNA in TGGA sequence context (**C**). The structural alignment of the central four base-pairs of the average structures of CP-DNA in AGGC and TGGA sequence contexts (**D**), OX-DNA in AGGC and TGGA sequence context (**E**) and CP- and OX-DNA in TGGA sequence context (F). Reproduced from Srinivas Ramachandran, Brenda R. Temple, Stephen G. Chaney and Nikolay V. Dokholyan, Structural basis for the sequence-dependent effects of platinum-DNA adducts. *Nucleic Acids Research* (2009) 37(8):2434-2448, with permission from Oxford University Press.

To further characterize the conformations sampled by CP- and OX-DNA adducts in the vicinity of platinum in the TGGA sequence context, we calculated the helical parameters of the central four base pairs of the dodecamer (T5G6G7A8) and the three

base-pair steps between them. With 6 parameters describing each base pair and 6 more for each base-pair step, there were a total of 42 helical parameters corresponding to the central four base pairs. We used the KS ratio (as described in Chapter 2) as a test for significant difference in comparing any two distributions of a particular helical parameter. To identify the parameters that showed major differences across different comparisons, we plotted the KS ratio of all the 42 parameters as a heat map. From the heat map, we selected the parameters that exhibited significant differences. When we compared the overall distributions of the helical parameters for CP-, OX- and undamaged DNA in the TGGA sequence context, both CP- and OX-DNA had significantly different conformations compared to undamaged DNA, especially in the G6-G7 base pair step, G6-C19 base pair and G7-C18 base pair (Figure 3.3). When comparing CP- and OX-DNA, we observed differences in T5-G6 slide, A8-T17 buckle, T5-A20 opening and G6-C19 opening (Figure 3.3). However, the differences between CP- and OX-DNA were minor, yielding KS ratios of ≤ 2. Thus, the CP- and OX-TGGA adducts appear to sample the same major DNA conformations when examined by this criteria.

3.2. The pattern and frequency of hydrogen bond formation between the drug and DNA depend both on the sequence context and carrier ligand

Earlier simulations in the AGGC sequence context had reported the formation of hydrogen bonds between platinum amines and adjacent bases (Sharma, et al., 2007), which correlated with minor conformational differences between CP- and OX-AGGC adducts that could influence the binding of HMGB1a to these adducts. We examined the trajectories of CP- and OX-TGGA adducts for hydrogen bond formation between all possible donors and acceptors using distance and angle criteria (as described in Chapter 2). In addition to the Watson-Crick hydrogen bonds in the DNA, we also observed the formation of hydrogen bonds between Pt-amines and adjacent base pairs.

When we compared the hydrogen bond patterns in the two sequence contexts, we observed that the bases involved and the frequency of formation of these hydrogen bonds were dictated both by the sequence context and the carrier ligand (Table 2.1).

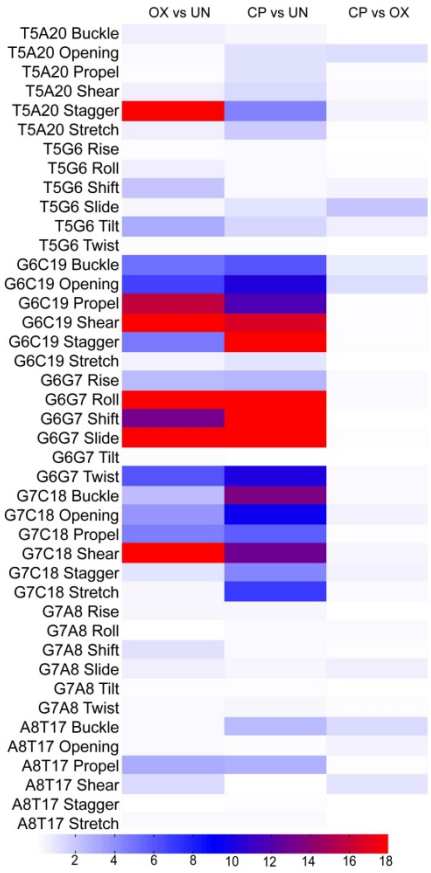

Figure 3.3. Conformational differences in overall distribution of helical parameters in the TGGA sequence context.
The conformational differences in the central four base pairs between CP-, OX- and undamaged DNA in the TGGA sequence context are represented as a KS heat map of 3 possible comparisons; OX-DNA vs undamaged DNA, CP-DNA vs undamaged DNA and CP- vs OX-DNA. The KS ratio decreases in the order of Red > Blue > White in the heat map.

In the AGGC sequence context, although the same hydrogen bonds were formed by both CP- and OX-Pt-amines, the frequency of hydrogen bond formation was different (Sharma, et al., 2007). The hydrogen bond to A5-N7 was formed more frequently for CP-DNA while the hydrogen bond to G7-O6 was formed more frequently for OX-DNA (Sharma, et al., 2007). In the TGGA sequence context, the G7-O6 hydrogen bond was formed by both CP- and OX-DNA and like in AGGC sequence

context, the G7-O6 hydrogen bond was formed more frequently by OX-DNA (Table 2.1). Other hydrogen bonds seen in the TGGA sequence context were unique to either CP- or OX-DNA. OX-DNA formed hydrogen bonds on the 5' side of the adduct, to T5-O3' but only for a small fraction of time (6%, Table 2.1). On the 3' side, CP formed hydrogen bond with A8-N7 with a frequency of 13% while OX formed hydrogen bonds with T17-O4 with a frequency of 15%. These hydrogen bond patterns in the TGGA sequence context that were unique to CP- and OX-DNA adducts (A8-N7 for CP-DNA, T17-O4 and T5-O3' for OX) all represented relatively minor conformations (occurring ≤ 15% of the time) of the Pt-DNA adduct.

Table 3.1. Frequency of formation of different hydrogen bonds between Pt Ammines and adjacent bases.

Reproduced from Srinivas Ramachandran, Brenda R. Temple, Stephen G. Chaney and Nikolay V. Dokholyan, Structural basis for the sequence-dependent effects of platinum-DNA adducts. *Nucleic Acids Research* (2009) 37(8):2434-2448, with permission from Oxford University Press.

TGGA			
CP		OX[a]	
Hydrogen bond type	Frequency	Hydrogen bond type	Frequency
G7-O6	32%	G7-O6	55%
A8-N7	13%	T17-O4	15%
		T5-O3'	6%
None	54%	None	23%
AGGC[b]			
CP		OX[c]	
G7-O6	13%	G7-O6	34%
A5-N7	40%	A5-N7	14%
A5-N7+G7-O6	34%	A5-N7+G7-O6	45%
None	13%	None	8%

[a]Only the equatorial hydrogen of the OX-amine was involved in hydrogen bonding on the 3' side of the adduct [b]from ref. [c]Both equatorial and axial hydrogens of the OX-amine were involved in hydrogen bonds on the 5' side, and only equatorial hydrogen of the OX-amine was involved in hydrogen bonding on the 3' side of the adduct

3.4. Platinum amines in OX are more constrained compared to CP

To determine the origin of differences between CP- and OX-DNA in the frequency of hydrogen bond formation with flanking bases on both sides of the Pt-GG adduct and their occupancy, we calculated the distributions of geometrical parameters of Pt from the simulations. As expected from the constraints imposed by the cyclohexane ring in OX, we observed that the 5'NH_x-Pt-3'NH_x bond angle had a significantly greater range for the CP-DNA adduct compared to the OX-DNA adduct (Figure 3.4) and the greater range for CP-DNA was observed in both TGGA and AGGC sequence contexts (data not shown). The 5'N7-Pt-5'NH_x and the 3'N7-Pt-3'NH_x bond angles also showed a slightly greater range for CP-DNA compared to OX-DNA (Figure 3.4). However, there was essentially no difference between CP- and OX-DNA in the 5'N7-Pt-3'N7 bond angle, presumably because of the constraints imposed by the DNA (Figure 3.4A). Thus, overall, CP-DNA was more flexible compared to OX-DNA with respect to the Pt-amines. The greater flexibility of CP compared to OX (especially with respect to the 5'NH_x-Pt-3'NH_x bond angle) may have resulted in the differences in local structure of the adduct, leading to differences in formation of hydrogen bonds between the drug and the adjacent bases.

To further characterize the differences in the flexibility of CP-amines and OX-amines, we examined the conformational flexibility of the N7-Pt-N-H dihedral angles for CP and OX on both 5' and 3' side of the adduct. The N7-Pt-N-H dihedral angle (Figure 3.5A-C) determines the orientation of the amine hydrogens, which influences the ability of those hydrogens to form hydrogen bonds with the adjacent bases. The N7-Pt-N-H dihedral angle for the CP-GG adduct has three broad peaks on both the 3' and 5' side of the adduct because all the hydrogens are equivalent and sample three different orientations. In contrast, the N7-Pt-N-H dihedral angle for OX has two relatively narrow peaks in distribution, with the one between -100º and -20º representing the equatorial hydrogen and the one between 20º and 80º representing the axial hydrogen in the 5'

amine. The peaks are reversed for the 3' amine. In both the AGGC sequence context (Figure 3.5D) and the TGGA sequence context (Figure 3.5E), the 3'N7-Pt-3'N-H dihedral angle positions the equatorial hydrogen of OX for the formation of the G7-O6 hydrogen bond, while the CP hydrogens are less frequently in the right orientation (compared to OX) for the formation of the G7-O6 hydrogen bond. Similarly in the TGGA sequence context, only the CP hydrogens spend a significant amount of time in a conformation favorable for the formation of the A8-N7 hydrogen bond and only the OX equatorial hydrogen spends a significant amount of time in a conformation favorable for the formation of the T17-O4 hydrogen bond (Figure 3.5E). Finally, in the AGGC sequence context, the 5'N7-Pt-N-H dihedral angle of CP allows one of the positions of the ammine hydrogens to be highly favorable for the formation of the A5-N7 hydrogen bond (Figure 3.5F) while the equatorial hydrogen in 5' side of OX has an orientation that is not as favorable as CP for the formation of the A5-N7 hydrogen bond. Thus, the allowable N7-Pt-N-H dihedral angles (in part determined by the carrier ligand) provides a structural basis for the type and frequency of hydrogen bond formed in CP- and OX-DNA adducts in the TGGA and AGGC sequence contexts.

3.5. Hydrogen bond formation is associated with distinctive distortions near the base to which the hydrogen bond is formed

To examine if hydrogen bond formation correlated with unique conformations in the central 4 base pairs in the TGGA sequence context, we calculated the KS ratios for the helical parameters of the central four base pairs associated with the different hydrogen bonded species. For both CP- and OX-DNA, structures forming G7-O6 hydrogen bond did not have major differences when compared to structures forming no hydrogen bonds to the Pt-amines (data not shown). However, we did observe significant differences when comparing the helical parameters of structures with CP-A8-N7

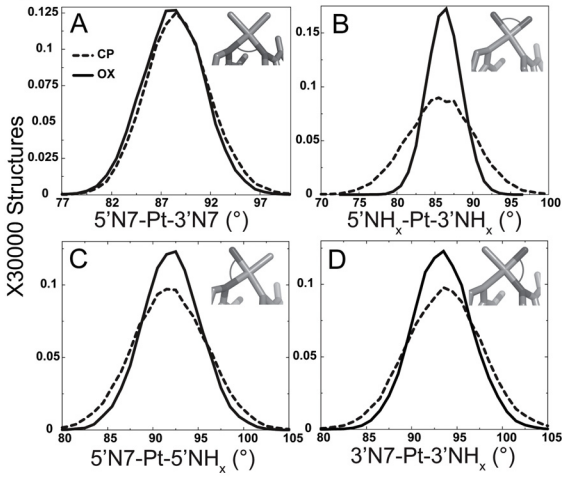

Figure 3.4. Geometrical parameters of platinum.
The distributions of the four angles around the square-planar platinum atom are plotted from the CP- and OX-TGGA simulations: 5'N7-Pt-3'N7 (**A**), 5'NH_x-Pt-3'NH_x (**B**), 5'N7-Pt-5'NH_x (**C**), 3'N7-Pt-3'NH_x (**D**). The Pt-amines at the 5' and 3' side of the adduct are denoted as 5'NH_x and 3'NH_x respectively. The N7s of G6 and G7 that are involved in covalent bonds with Pt are denoted as 5'N7 and 3'N7 respectively. Reproduced from Srinivas Ramachandran, Brenda R. Temple, Stephen G. Chaney and Nikolay V. Dokholyan, Structural basis for the sequence-dependent effects of platinum-DNA adducts. *Nucleic Acids Research* (2009) 37(8):2434-2448, with permission from Oxford University Press.

hydrogen bond to structures with the CP-G7-O6 hydrogen bond and in comparing structures with OX-T17-O4 hydrogen bond to structures with OX-G7-O6 hydrogen bond (Figure 3.6). From the KS ratio map of comparison of structures with the CP-A8-N7 hydrogen bonds to the structures with the CP-G7-O6 hydrogen bond (Figure 3.6A), we observed the greatest differences in the G7-A8 base pair step, especially in rise, roll, shift, twist and slide parameters. Significant differences were also observed for G6-G7 shift and G6-C19 opening. The parameters with major differences between structures with CP-A8-N7 hydrogen bond and all other species in CP-DNA yielded KS ratios of ~8-15 indicating that the CP-A8-N7 hydrogen bonded species had a unique conformation compared to all other species in CP-DNA. Similarly, we observed from the KS ratio map of comparison of structures with OX-T17-O4 hydrogen bond to structures with OX-G7-O6 hydrogen bond (Figure 3.6A) that the formation of OX-T17-O4 hydrogen bond resulted in unique conformations at G7-C18 base pair, G7-A8 base pair step and A8-T17 base pair, as seen in G7-C18 shear, stagger and stretch; G7-A8 slide and A8-T17

buckle parameters. A significant difference was also observed for the G6-G7 twist. The same differences were also seen when the helical parameters were compared for structures with the OX-T17-O4 hydrogen bond to structures with no hydrogen bonds (data not shown).

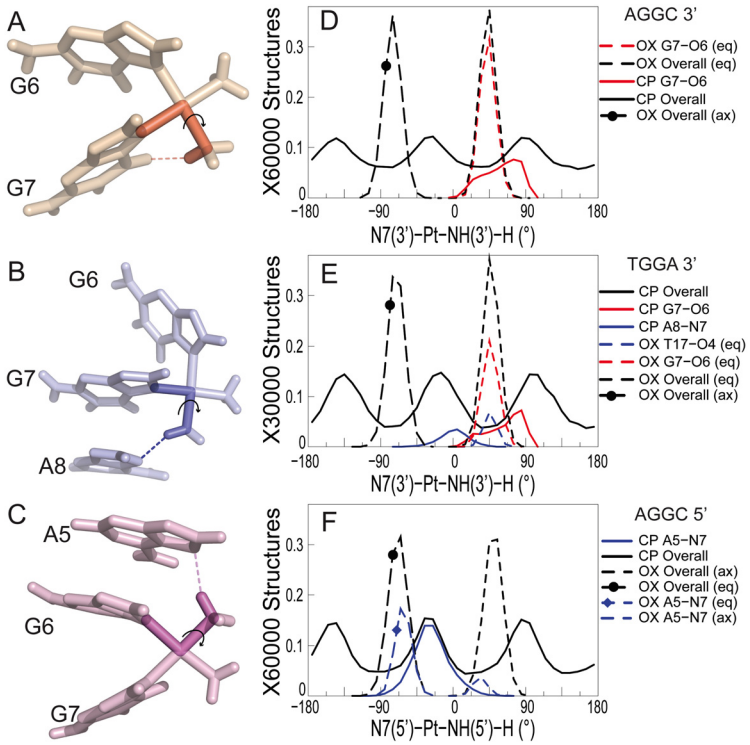

Figure 3.5. Dihedral angle involved in hydrogen bond formation.
The dihedral angle describing the Pt-amine hydrogen orientation while forming hydrogen bond with adjacent DNA bases is shown for the G7-O6 hydrogen bond in CP-DNA in the AGGC sequence context (A), the A8-N7 hydrogen bond in CP-DNA in the TGGA sequence context (B) and the A5-N7 hydrogen bond in CP-DNA in the AGGC sequence context (C) respectively. Oxaliplatin has two hydrogens for each Pt-Ammine – equatorial (eq) and axial (ax). The distribution of the 3'N7-Pt-NH_x-H dihedral angle is shown for the AGGC sequence context (D) and the TGGA sequence context (E). The distribution of the 5'N7-Pt-NH_x-H dihedral angle is shown for the AGGC sequence context (F). Reproduced from Srinivas Ramachandran, Brenda R. Temple, Stephen G. Chaney and Nikolay V. Dokholyan, Structural basis for the sequence-dependent effects of platinum-DNA adducts. *Nucleic Acids Research* (2009) 37(8):2434-2448, with permission from Oxford University Press.

The distributions of helical parameters of the hydrogen-bonded species showing major differences in CP-DNA and OX-DNA are plotted in Figure 3.6B and Figure 3.6C, respectively. The G6G7A8 portion of the centroid structures forming the CP-A8-N7/OX-T17-O4 hydrogen bond is compared with CP-G7-O6/OX-G7-O6 hydrogen bond in

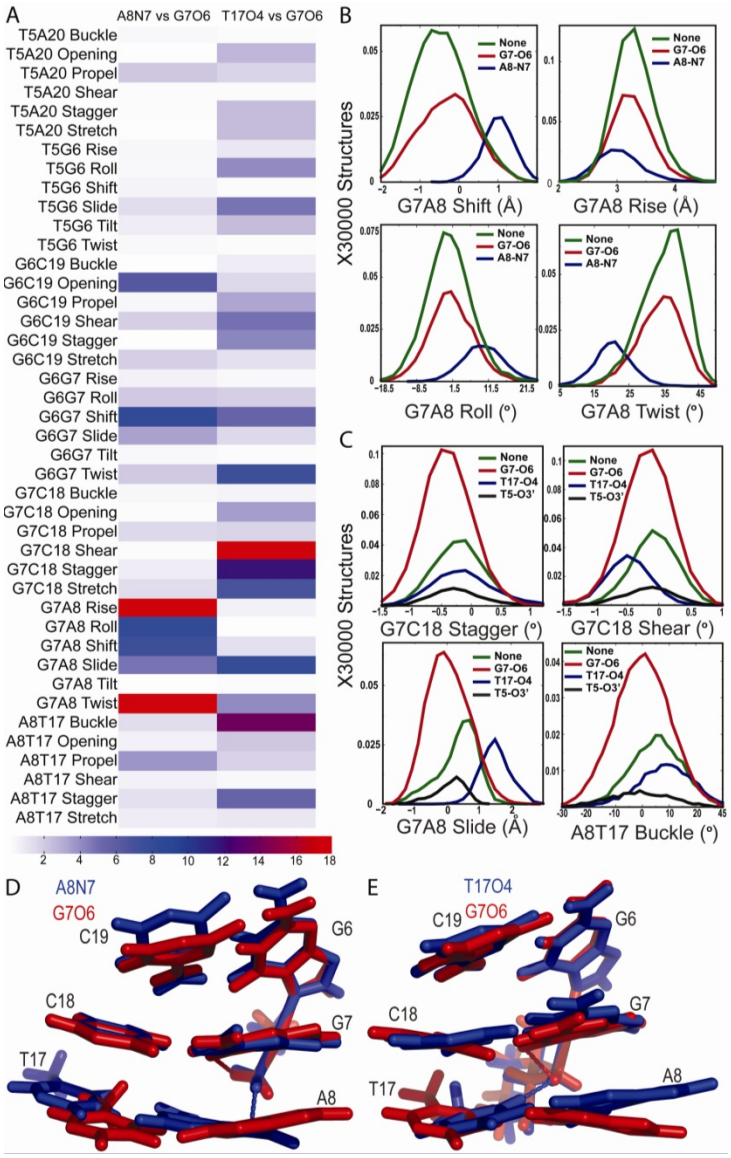

Figure 3.6. Helical parameters in the TGGA sequence context.
The conformational differences between two hydrogen-bonded species in all the 42 parameters are shown in a heat map (**A**). We represent the differences as the KS ratio, which is color-coded (The KS ratio decreases in the order of Red > Blue > White). Plots of histograms of the four helical parameters showing significant differences for different hydrogen bonded species of CP-DNA adduct (**B**) and OX-DNA adduct (**C**), are shown. Alignment of 5'G6G7A8 3' base pairs of the centroid structures forming the CP-G7-O6 hydrogen bond (red) and the CP-A8-N7 hydrogen bond (blue) (**D**) are shown. Alignment of 5'G6G7A8 3' base pairs of the centroid structures forming the OX-G7-O6 hydrogen bond (red) and the OX-T17-O4 hydrogen bond (blue) (**E**) are also shown. The structures are aligned based on Pt-G6G7. Reproduced from Srinivas Ramachandran, Brenda R. Temple, Stephen G. Chaney and Nikolay V. Dokholyan, Structural basis for the sequence-dependent effects of platinum-DNA adducts. *Nucleic Acids Research* (2009) 37(8):2434-2448, with permission from Oxford University Press.

Figure 3.6D and Figure 3.6E, respectively. In summary, we found that the formation of the minor hydrogen bonds on the 3' flanking base pair in CP- and OX-DNA

was associated with unique conformations in the 3' side of the adduct. We do not describe here the helical parameters of structures with T5-O3' hydrogen bond in OX-DNA since this hydrogen bond was formed only in 6% of the structures and because binding of HMGB1a to Pt-DNA is primarily through interactions on the 3' side of the adduct.

3.6. OX T17-O4 and CP A8-N7 are conformationally distinct with respect to the minor groove

Formation of unique hydrogen bonds by CP- and OX-DNA to the drug suggested that these hydrogen-bonded species could represent structural differences between CP- and OX-DNA. When we compared structures forming the CP-A8-N7 hydrogen bond to structures forming the OX-T17-O4 hydrogen bond, we did observe significant differences. When seen facing the minor groove, the formation of CP-A8-N7 hydrogen bond shifted the A8-T17 base pair towards the left, while the formation of OX-T17-O4 hydrogen bond shifted the A8-T17 base pair to the right (Figure 3.7A). Thus, the structural distortions associated with the formation of these hydrogen bonds are in opposite directions with reference to the minor groove. Analyzing these differences quantitatively using helical parameters, we observed that the mean value of G7-A8 slide is -1 Å for the CP-A8-N7 hydrogen bond, while it is +1.8 Å for the CP-T17-O4 hydrogen bond (Figure 3.7B). Similarly, the shift, twist and roll of the G7-A8 base pair step are clearly different for structures with CP-A8-N7 hydrogen bond compared to those with the OX-T17-O4 hydrogen bond (Figure 3.7B). As might be expected, these conformational differences correlated with the T17-O4 atom being closer to the Pt-amine hydrogen of OX and the A8-N7 atom being closer to the Pt-amine hydrogen of CP. In summary, when comparing CP-DNA to OX-DNA, the minor conformations had distinct distributions

of helical parameters in the vicinity of hydrogen bond formation that were unique to either CP- or OX-DNA.

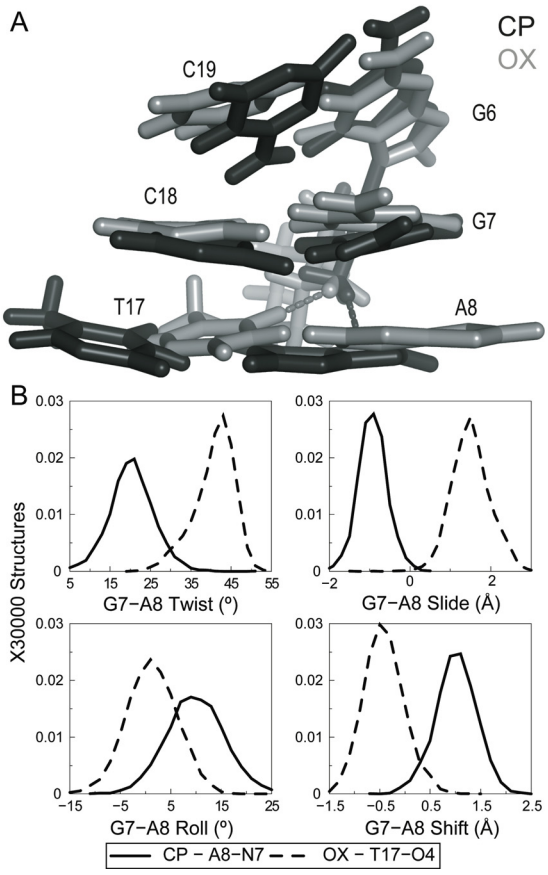

Figure 3.7. Differences in DNA conformation and helical parameters of A8-N7 and T17-O4 hydrogen bonded species in CP- and OX-DNA respectively.
(A) Alignment of the 5'G6G7A8 3' base pairs of the centroid structures forming A8-N7 hydrogen bond in CP-DNA adduct and the T17-O4 hydrogen bond in the OX-DNA adduct is shown. The structures are aligned based on Pt-G6G7. (B) Plots of histograms of the four helical parameters showing greatest differences between the A8-N7 hydrogen bonded species in CP-DNA and T17-O4 hydrogen bonded species in OX-DNA are shown. The distributions of twist, slide, roll and shift parameters of the G7-A8 base-pair step are plotted because the greatest differences are in this base-pair step (data not shown). The solid line represents distribution of structures with CP-A8-N7 hydrogen bond while the dashed line represents distribution of structures with OX-T17-O4 hydrogen bond. The frequency distributions are calculated and normalized as described earlier. Reproduced from Srinivas Ramachandran, Brenda R. Temple, Stephen G. Chaney and Nikolay V. Dokholyan, Structural basis for the sequence-dependent effects of platinum-DNA adducts. *Nucleic Acids Research* (2009) 37(8):2434-2448, with permission from Oxford University Press.

3.7. Conclusions

Our simulations of Pt-DNA in the TGGA sequence context provide the first glimpse of distinct conformations sampled by CP- and OX-DNA. Our extensive simulations show little differences between the major conformations sampled by CP- and OX-DNA, which agrees well with data from X-ray crystallography in the TGGT sequence context and NMR spectroscopy in the AGGC sequence context. However, we also report distinct hydrogen bonds in CP- and OX-DNA formed between Pt-amines and the base pairs adjacent to the GG-adduct. The distinct hydrogen bonds correlate with distinct conformations on the 3' side of the adduct. Here, it is important to note that we cannot determine if it is the hydrogen bonds that drive distinct conformations. However, these hydrogen bonds offer a unique signature that is used to separate minor conformations in our simulation ensemble. The fact that these hydrogen bonded species have specific conformational characteristics underscores the robustness of using Pt-amine-DNA hydrogen bonds to uncover minor conformations. In summary, we find that indeed, it is the conformational dynamics and the minor conformations sampled by CP- and OX-DNA that differentiate the adducts in the TGGA sequence context. These conformational differences, especially on the 3' side of the adduct might be important in differential binding affinity of HMGB1a, since the protein's binding mode to Pt-DNA orients it to the 3' side of the adduct. In subsequent chapters, we will explore the effect of these conformational differences in protein recognition and binding.

Chapter 4. Effect of sequence context on the conformational dynamics of Pt-DNA adducts

The sequence dependence on the extent of differential binding of proteins to CP- and OX-DNA (Table 3.1) suggests sequence context dependent differences in structural distortions caused by CP- and OX-GG adducts. Even though DNA by itself has several sequence dependent structural features that are exploited by proteins that bind DNA in a sequence dependent manner, the presence of Pt adduct bestows additional interactions and distortions, the extent of which could depend on the bases flanking the Pt-GG adduct. MD simulations on CP- and OX-DNA adducts performed in an identical manner in three different sequence contexts allows us to compare the effect of both carrier ligand and sequence context on the conformational dynamics of DNA.

4.1. DNA conformation in the vicinity of the Pt-GG adducts

In the context of the undamaged DNA, TGGA and TGGT sequences would be expected to have similar conformations in the 5' side of the GG adduct, while AGGC sequence will have some unique conformational signatures. On the 3' side, TGGA is more different than AGGC and TGGT because of a purine on the 3' side of the adduct as opposed to pyrimidines in the other sequences. The differences in the undamaged DNA could either be maintained in Pt-DNA or be overtaken by the distortions due to Pt-adduct. Additionally, sequence dependent differences can arise in Pt-DNA that were not seen in undamaged DNA.

To understand the effect of Pt adduct and the sequence context on DNA conformation near the adduct, we compared the helical parameters corresponding to the central four base-pairs from our simulations in the TGGA, TGGT and AGGC sequence context. We observed significant differences between the three sequences in either undamaged or CP- or OX-DNA in 17 of the 42 helical parameters, indicating large-scale conformational dependence on sequence context (with or without the drug). We further classify these parameters into four groups that are characterized by:

Group 1: Differences that are consistent across undamaged, CP- and OX-DNA

Group 2: Differences in undamaged DNA that are suppressed by the presence of Pt adduct

Group 3: Differences that are brought about due to the presence of Pt adduct, and may be specific to CP- or OX-DNA

Group 4: Differences that can be predominantly explained as due to the occurrence of hydrogen bonds between Pt-amines and adjacent DNA bases

The ability to define these groups allows us to delineate sequence-dependent effects (Group 1), Pt-dependent effects (Group 2), carrier ligand dependent effects (Group 3) and effects dependent on both carrier ligand and sequence context (Group 4). We will discuss the conformational parameters that fall into these groups next.

Group1. The differences in the group are in the 5' side of the adduct and AGGC sequence is observed to be different compared to TGGA and TGGT sequences that are similar to each other. Thus, the sequence dependent changes in undamged DNA by having and adenine compared to thymine on the 5' side of the adduct are maintained in 5-20 buckle, 5-6 roll and 5-6 tilt. AGGC sequence features mean positive buckle, while TGGA and TGGT sequences feature mean negative buckle in the base-pair 5' to the

adduct (Figure 4.1). The similar trend is maintained in the presence of CP and OX adducts. Similarly, the roll on the 5' base-pair step is lower in AGGC compared to TGGA and TGGT (Figure 4.1), while AGGC features a mean negative tilt compared to TGGA and TGGT sequences. No such significant differences were seen in the 3' side of the adduct.

Group 2. Similar to Group1, AGGC sequence in the undamaged DNA is different to TGGA and TGGT sequences in 5-6 shift, rise and twist, 6-7 shift and 8-17 propel. However, in the presence of Pt-adduct, these significant differences in undamaged DNA disappear, imposing a homogeneity in these helical parameters (Figure 4.2).

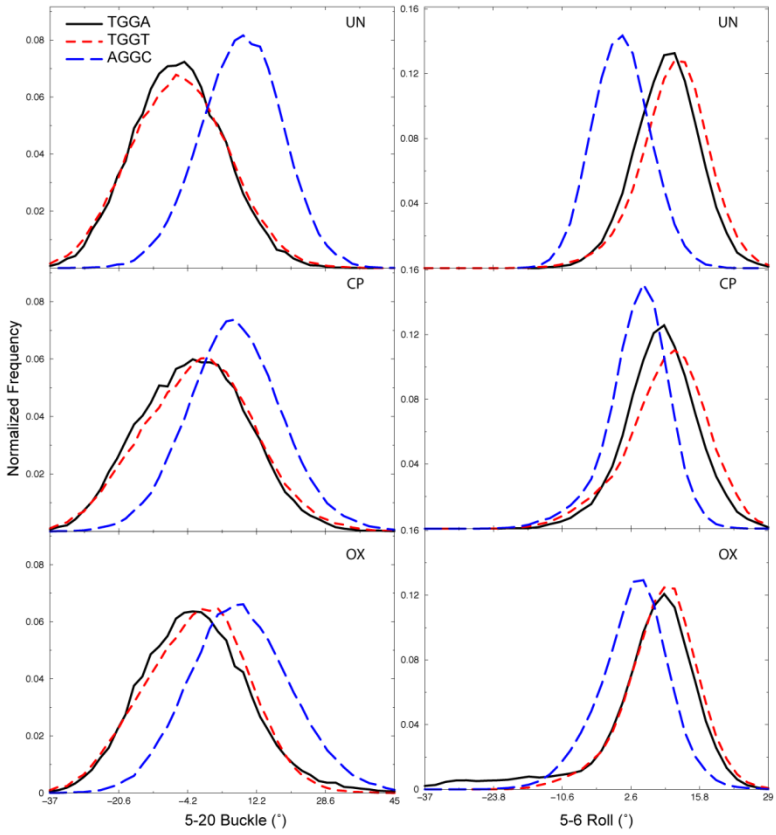

Figure 4.1. Helical parameters having similar trends in undamaged, CP- and OX-DNA when compared across AGGC, TGGA and TGGT sequence contexts.
Not shown here are the distributions for 5-6 tilt.

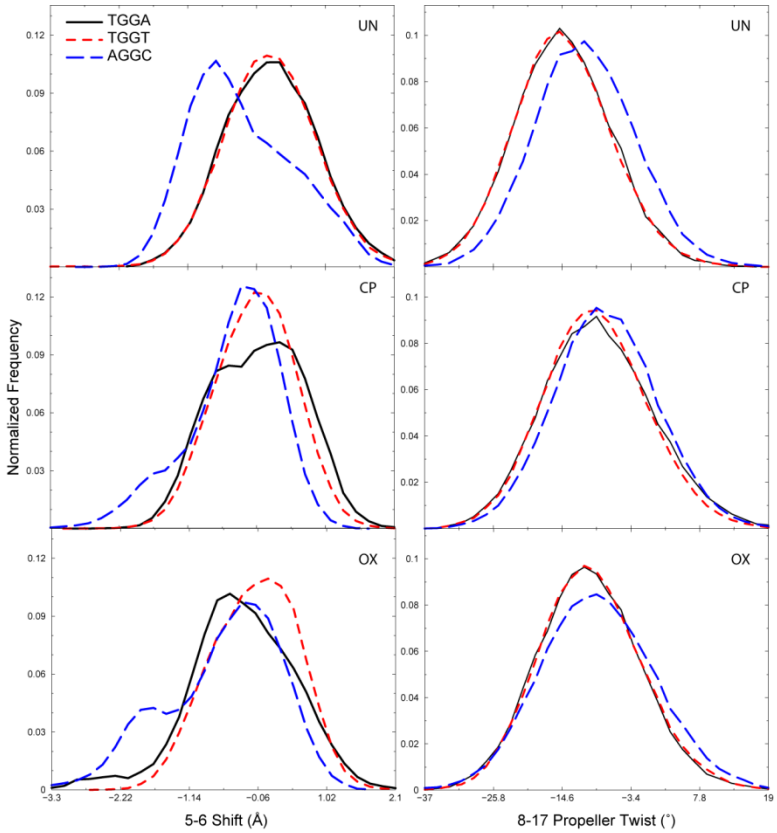

Figure 4.2. Helical parameters in which the sequence-specific conformation in undamaged DNA is suppressed in CP- and OX-DNA.

Group 3. This group is characterized by helical parameters that show no significant difference in undamaged DNA, but presence of CP and OX adducts induces sequence-specific changes. These changes are either similar in CP and OX or are carrier ligand specific. Thus, this group signifies Pt and carrier ligand specific conformation in a given sequence. We observe this trend in 5-20 propeller twist, 6-19 buckle and propeller twist, 7-18 buckle, stagger and propeller twist, and 7-18 stagger. 5-20 propeller twist illustrates this group well: AGGC has a lower 5-20 propeller twist in both CP- and OX-DNA, while TGGT sequence has lower 5-20 propeller twist in CP-DNA. TGGA features uniform values for the 5-20 propeller twist. Other parameters also feature similar differences that are specific for CP- and OX-DNA, with some examples shown in Figure 4.3.

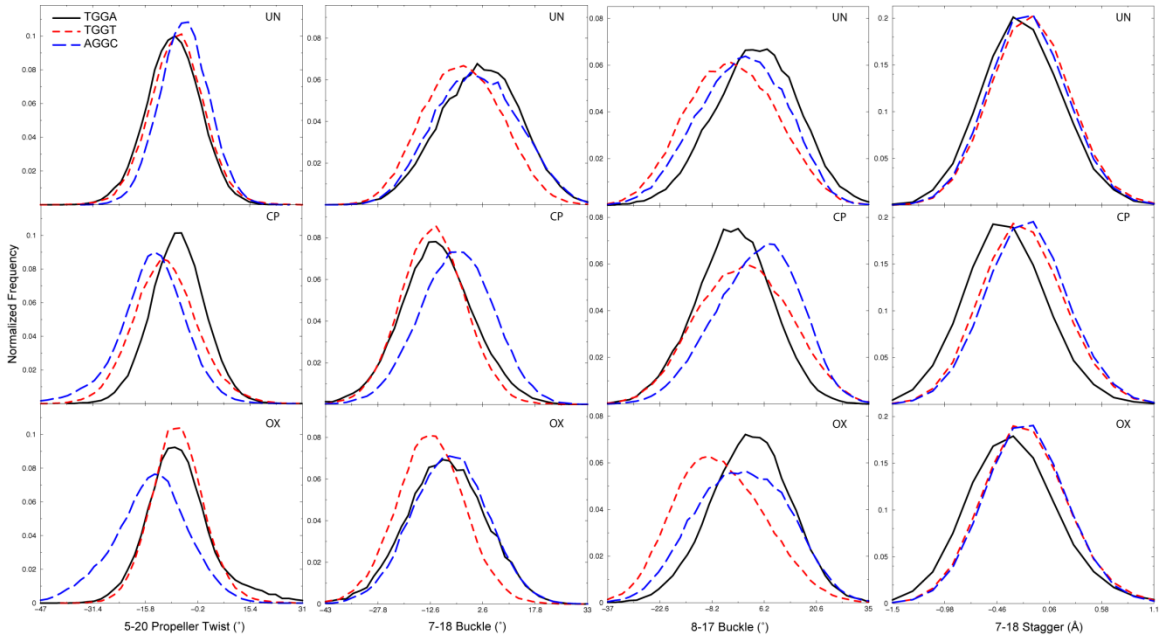

Figure 4.3. Helical parameters in which the presence of Pt-adduct induces differences between different sequences, which may be carrier ligand specific.

Group 4. This group is a subset of Group 3, but here we know that the sequence and carrier ligand specific conformations are accompanied by hydrogen bonding between Pt-amine and the adjacent base. There are only two parameters where these differences show up: 5-6 slide and 7-8 slide. Hydrogen bonding between A5 and 5' Pt-amine leads to negative values of 5-6 slide in the CP- and OX-DNA in the AGGC sequence context compared to TGGA and TGGT sequence context, where the value of this parameter in Pt-DNA mirrors closely to undamaged DNA. CP-DNA in TGGT sequence context has a shoulder at positive values of the slide, which does represent a minor conformation, but this conformation is not accompanied by any specific hydrogen bond. In the TGGA sequence context, as seen in Chapter 3, CP- and OX-DNA form distinct hydrogen bonds with the 3' flanking base-pair – CP-DNA forms the A8N7 hydrogen bond, while OX-DNA forms the T17O4 hydrogen bond. Also, as seen in Chapter 3, the formation of these hydrogen bonds lead to a positive value of the 7-8 slide in OX-DNA and a negative slide in the CP-DNA. These minor conformations skew the overall distribution of the 7-8 slide in opposite directions in CP- and OX-DNA with

respect to the other sequences. AGGC on the other hand shows a more negative slide in undamaged DNA, but is quite similar to the TGGT sequence in Pt-DNA (Figure 4.4).

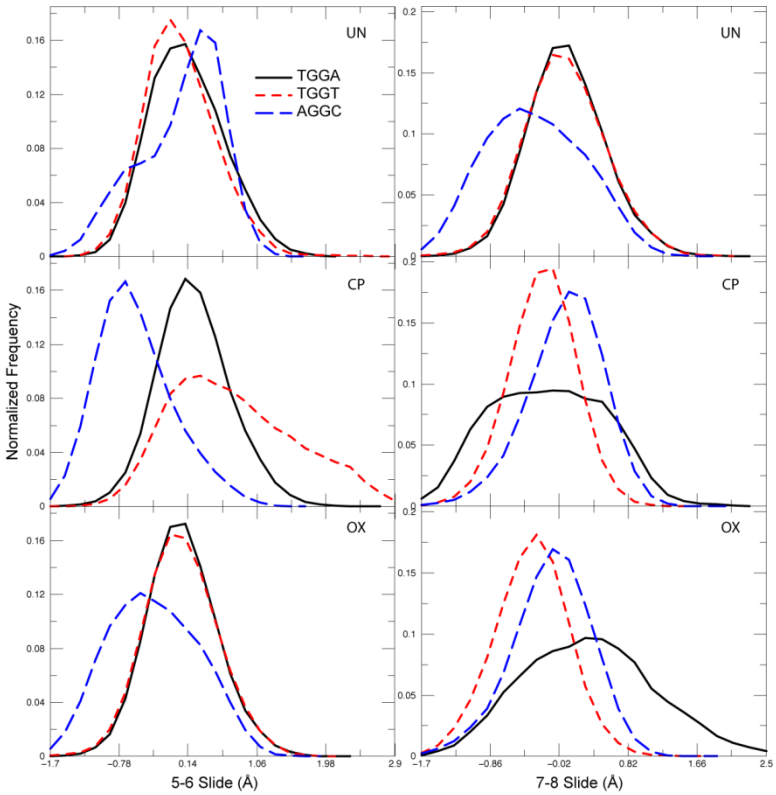

Figure 4.4. Helical parameters showing sequence-specific conformations in Pt-DNA that are accompanied by hydrogen bonding between Pt-amine and base-pair adjacent to the Pt-GG adduct.

4.2. Hydrogen bond formation between Pt amines and adjacent base-pairs

In chapter 3, we discussed the formation of hydrogen bonds between Pt-amines and adjacent bases in our simulations of Pt-DNA. These hydrogen bonds are observed in all three sequence contexts we have performed simulations with (AGGC, TGGA, TGGT). In the TGGT sequence context, we observe two types of hydrogen bonds formed between Pt-amines and DNA in both CP- and OX-DNA. The hydrogen bond between the 3' Pt-amine and the O6 atom of the 3' Guanine (the G7-O6 hydrogen bond) is formed more frequently by OX-DNA (72% of the time compared to 32% by CP-DNA, Table 4.1), while the hydrogen bond between the 3' amine and the O4 atom of 3'

Thymine (the T8-O4 hydrogen bond) is formed more frequently by CP-DNA (49% compared to 19% by OX-DNA). When we consider the hydrogen bond patterns from three different sequence contexts and two carrier ligands, we observe both carrier ligand and sequence-specific differences (Table 4.1).

Table 4.1. Frequency of formation of different hydrogen bonds between Pt Ammines and adjacent bases

TGGT			
CP		OX[a]	
Hydrogen bond type	Frequency	Hydrogen bond type	Frequency
G7-O6	20%	G7-O6	59%
T8-O4	37%	T8-O4	6%
T8-O4+G7-O6	12%	T8-O4+G7-O6	13%
None	29%	None	20%
TGGA			
CP		OX[a]	
G7-O6	32%	G7-O6	55%
A8-N7	13%	T17-O4	15%
		T5-O3'	6%
None	54%	None	23%
AGGC[b]			
CP		OX[c]	
G7-O6	13%	G7-O6	34%
A5-N7	40%	A5-N7	14%
A5-N7+G7-O6	34%	A5-N7+G7-O6	45%
None	13%	None	8%

The first carrier ligand specific trend we observe is that the formation of a hydrogen bond between the 3' Pt-amine and G7-O6 (O6 atom of the 3' Guanine in Pt-GG) occurs more frequently for OX-DNA adducts than for CP-DNA adducts in all three

sequence contexts. This trend is mainly due to the hydrogens of Pt-amines in OX being locked in an orientation most favorable for the formation of the G7-O6 hydrogen bond, while those in CP are free to move, spending much lesser time in the orientation required for the G7-O6 hydrogen bond (Figure 3.5). The second carrier ligand specific effect we observe is that the ease of formation of hydrogen bonds between Pt-amines and bases adjacent to the GG adduct (the 5'A in the AGGC sequence context and the 3'T or 3'A in the TGGT and TGGA sequence contexts) is higher for CP-DNA adduct compared to the OX-DNA adduct. Presumably, this effect is also the consequence of the constraints placed on the amine by the cyclohexane ring of OX.

In terms of sequence-specific effects, we observe that significant frequency of hydrogen bonding on the 5' side of the adduct occurs only in the AGGC sequence context (the A5-N7 hydrogen bond). Given the structural characteristics of a double helix, only the N7 atoms of adenine and guanine are accessible for hydrogen bond formation by the 5' Pt-ammine and no significant hydrogen bonding is seen when the 5' base is thymine. Apart from the G7-O6 hydrogen bond, similar hydrogen bonds are formed by Pt-amines to the adjacent bases in AGGC and TGGT sequence contexts. However, in the TGGA sequence context, the hydrogen bond formed by the Pt-amine (other than G7-O6) is unique to CP- and OX-DNA. CP-DNA forms the A8-N7 hydrogen bond on the 3' side of the adduct. OX-DNA cannot form a hydrogen bond with A8-N7, but is able to form a hydrogen bond with O4 of the thymine on the opposite strand. The distinct hydrogen bonds formed in the TGGA sequence context correlate with the highest differences in differential binding affinities for CP- and OX-GG adducts by HMGB1a, HMGB1b and TBP(Wei, et al., 2001). Thus, we observe that the hydrogen bond formation significantly correlates with the pronounced sequence dependent effects of Pt-DNA adducts as observed from MD simulations and may point to minor

conformations of Pt-DNA adducts that influence the recognition of the adducts by DNA binding proteins.

4.3. Conclusions

From our comparison of DNA conformation in the vicinity of the Pt-GG adduct, we can conclude that the conformation of CP- and OX-GG adducts depend a lot on the flanking bases. We observed several helical parameters being influenced in a carrier-ligand and sequence dependent manner. These conformational differences could be the origin of the observed sequence dependence in binding of proteins and the efficiency of translesion polymerases. Specifically, most of the distinct conformations in the 5' side are seen in the AGGC sequence context, while many differences in the 3' side are seen in both TGGT and TGGA sequence contexts. The formation of sequence-dependent hydrogen bonds by Pt-amines reflect not only the differences in the electron donor in the bases adjacent to the Pt-GG adduct, but also the difference in flexibility that leads to hydrogen bonds either on the 5' side or the 3' side of the adduct. Finally it is worth noting that several sequence dependent structural features of undamaged DNA are suppressed by the formation of Pt-GG adduct, indicating the overwhelming structural distortion induced by Pt.

Chapter 5. Interaction of HMGB1a with Pt-DNA

As elaborated in Chapter 1, differential binding of CP- and OX-DNA to HMG-domain proteins could be an important facet of differential efficacies of CP and OX in different tumors. More importantly, HMG-domain proteins have been shown to play important role in Pt drug sensitivity. HMGB1 is one of the first identified proteins to bind to Pt-DNA adducts and hence has been characterized in detail. Furthermore, the crystal structure of HMGB1a-Pt-DNA is available only for CP-DNA in the TGGA sequence context (PDB ID 1CKT (Ohndorf, et al., 1999)). To uncover the basis for differential binding affinity, structural data is required for both CP- and OX-DNA binding to HMGB1a. In this scenario, MD simulations are able to provide structural details of HMGB1a binding to both CP- and OX-DNA. We performed three sets of simulations of 50 ns each of the complex between HMGB1a and Pt-DNA in three sequence contexts (TGGA, TGGT and AGGC) and with two drugs (CP and OX). With these simulations, our goal was to uncover the molecular basis of ~53 fold difference in binding affinity between CP- and OX-DNA in the TGGA sequence context and also the sequence dependent interactions of HMGB1a with Pt-DNA. We observed that these simulations showed uniform RMSD fluctuations after about five nanoseconds; hence we utilized the final 45 ns of all the trajectories for various structural analysis.

5.1. DNA conformational parameters that influence HMGB1a binding

We have discussed that one of the most important determinants of HMGB1a binding was the effective intercalation of Phe37 between the platinated GG basepair

step. Additionally, it is known that HMGB1a binds efficiently to bent DNA, in fact the binding affinity of HMGB1 to DNA minicircles is similar to that of Pt-DNA (Webb, et al., 2001). The crystal structure of HMGB1a-Pt-DNA also revealed a hydrogen bond between Ser41 in HMGB1a and the base 5' to the Pt-GG adduct. Finally, the crystal structure revealed multiple interactions between the HMGB1a binding interface and the minor groove of Pt-DNA. The conformation of DNA plays an important role in determining the efficiency of the Phe37 intercalation, Ser41 hydrogen bond and efficient bending of DNA by HMGB1a binding, which provides a wide and shallow minor groove suitable for interacting with HMGB1a binding interface. Thus, in this section we will analyze the conformation of bound and free Pt-DNA in the context of these three parameters.

5.1.1. Conformations favoring Phe37 stacking

Binding of HMB1a to Pt-DNA involves the intercalation of Phe37 in the platinated base-pair step, resulting in the roll of this base-pair step being 56.7º (Ohndorf, et al., 1999). Thus, ability to sample higher roll could result in better binding affinity of Pt-DNA. The G6-G7 base pair step has a mean roll of 3.3º and 5.3º in undamaged DNA in the TGGA and AGGC sequence contexts respectively. The formation of either CP- or OX-G6G7 adducts shifted the G6-G7 roll to significantly higher values compared to undamaged DNA (Figure 5.1). There was also a pronounced shoulder in the distributions of G6G7 roll parameters in Pt-DNA adducts in both TGGA and AGGC sequence contexts (Figure 5.2). This shoulder lies in the region that is favorable for binding of HMGB1a, and differs between CP- and OX-GG adducts to different extents in different sequence contexts. In the TGGA sequence context, the CP-GG adduct explored conformations with G6G7 roll ±10º of the roll of CP-DNA bound to HMGB1a 3.2 times more frequently than OX-GG adducts, while in the AGGC sequence context, CP-

and OX-GG adducts explored rolls within ±10º of the roll of CP-DNA bound to HMGB1a to about the same extent. The distributions with higher roll were mainly comprised of structures forming the CP-A8-N7 hydrogen bond in the TGGA sequence context (Figure 5.2), while in the AGGC sequence context, the regions of high roll were associated mainly with the formation of both CP- and OX-A5-N7 hydrogen bond (Figure 5.2). Thus, hydrogen bonding to adjacent adenine in both sequence contexts was associated with higher roll in the G6G7 base pair step.

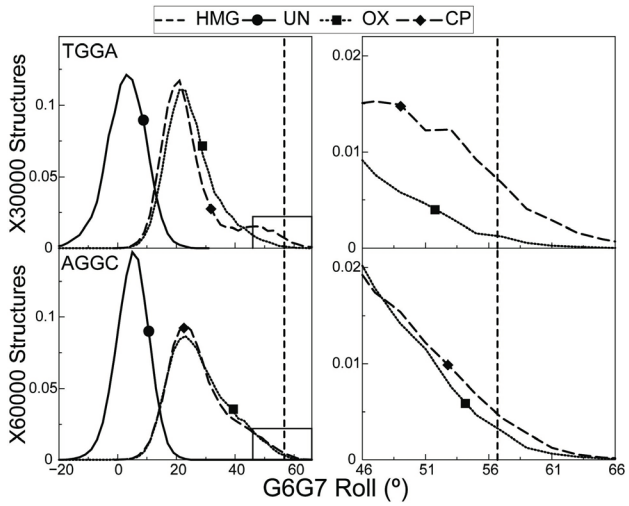

Figure 5.1. Distribution of the G6-G7 roll.
The distribution of G6-G7 roll, which is important for intercalation of Phe37 of HMGB1a between the G6-G7 base pair step is plotted for the AGGC and the TGGA sequence contexts. The distributions of CP-, OX- and undamaged DNA are plotted in each sequence context. The bend angle of DNA in the crystal structure of CP-DNA bound to HMGB1a(Ohndorf, et al., 1999) is plotted as a vertical dashed line. The region of roll ±10º of the roll in the crystal structure of CP-DNA bound to HMGB1a is plotted alongside to highlight differences between CP- and OX-DNA in the TGGA sequence context. Reproduced from Srinivas Ramachandran, Brenda R. Temple, Stephen G. Chaney and Nikolay V. Dokholyan, Structural basis for the sequence-dependent effects of platinum-DNA adducts. *Nucleic Acids Research* (2009) 37(8):2434-2448, with permission from Oxford University Press.

The difference between CP- and OX-DNA in the roll of the G6-G7 base-pair step may be significant for HMGB1a binding to Pt-DNA adducts. Ohndorf *et al* (Ohndorf, et al., 1999) have shown that the crystal structure of the HMGB1a-CP-DNA complex has significantly greater roll (56.7º) at the platinated GG base pair step than free CP-DNA and have postulated that the greater roll enables ideal geometry for π-π stacking of

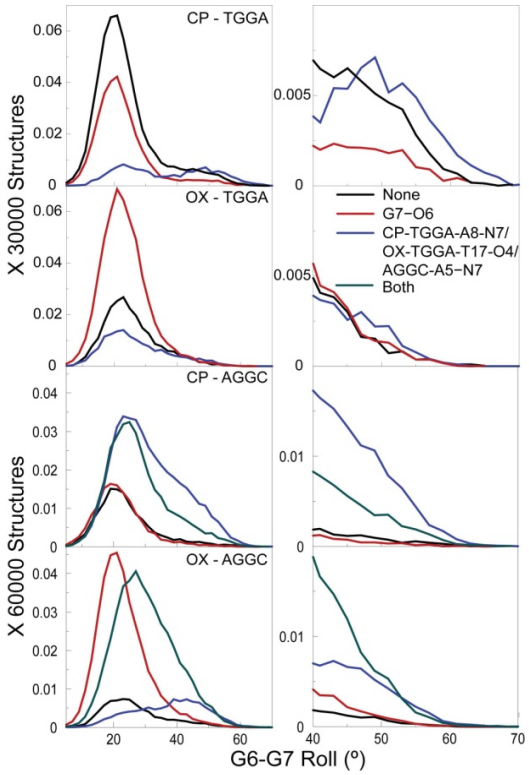

Figure 5.2. G6-G7 roll parameter of different hydrogen bonded species in CP- and OX-DNA adducts in the TGGA and AGGC sequence contexts.
The distribution of G6-G7 roll of different hydrogen-bonded species in CP-TGGA, OX-TGGA, CP-AGGC and OX-AGGC are plotted. The left panel shows the distribution for the whole range of roll values, while the right panel is zoomed into the distributions at roll > 40°.

Phe37 of HMGB1a with the 3' Guanine of the platinated base-pair step. This interaction appears to be particularly important for the stability of the HMGB1a-Pt-DNA complex, since the Phe37Ala mutation reduces binding affinity >667-fold. The ability of free CP-DNA in the TGGA sequence context and both free CP- and OX-DNA in the AGGC sequence context (but not free OX-DNA in the TGGA sequence context) to sample roll at values seen in the crystal structure of the HMGB1a-CP-DNA complex would suggest that these Pt-DNA adducts have the conformational flexibility to readily form the HMGB1a-Pt-DNA complex. In contrast, OX-TGGA alone samples lower roll angles at the platinated base-pair step, suggesting that it would have more difficulty forming a complex that has optimal stacking of Phe37 to the 3'G. As expected, our simulations of the HMGB1a complexes with Pt-DNA show that indeed the mean platinated base-pair

roll of OX-TGGA is downshifted by ~3.2º compared to the roll seen in CP- and OX-AGGC and CP-TGGA and in the crystal structure of the HMGB1a-CP-DNA complex (Figure 5.3).

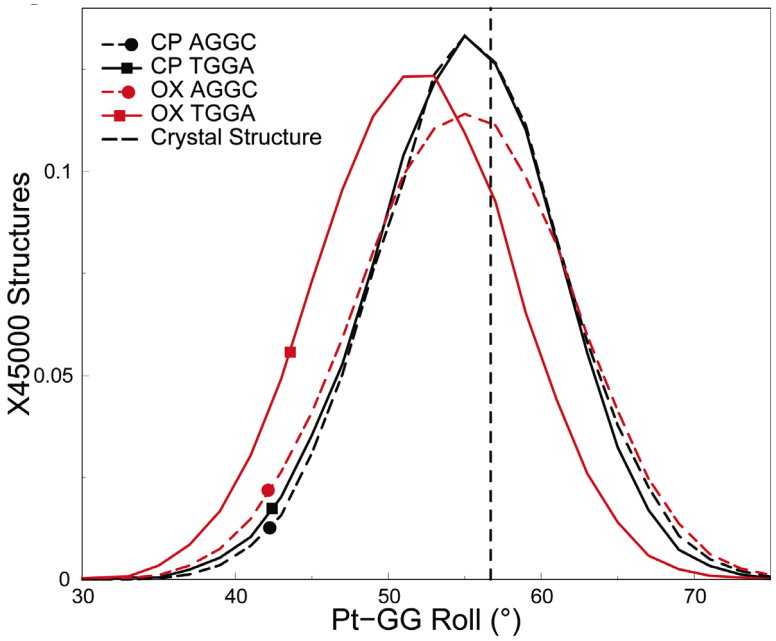

Figure 5.3. Distributions of the Pt-GG roll in the HMGB1a-Pt-DNA simulations.
The distribution of the roll of the Pt-GG base-pair step, which is important for stacking of Phe37 of HMGB1a to the 3'G is plotted for the HMGB1a-Pt-DNA complexes in the AGGC and the TGGA sequence contexts. The dashed vertical line represents the roll of the G6-G7 base pair step from the HMGB1a-CP-DNA crystal structure. Reproduced from Srinivas Ramachandran, Brenda R. Temple, Stephen G. Chaney and Nikolay V. Dokholyan, Structural basis for the sequence-dependent effects of platinum-DNA adducts. *Nucleic Acids Research* (2009) 37(8):2434-2448, with permission from Oxford University Press.

In summary, CP-DNA in the TGGA sequence context was able to sample conformations that resulted in a high roll in the G6G7 base pair step, which has been suggested to favor binding to HMGB1a (Ohndorf, et al., 1999), while OX-DNA in the same sequence context was unable to sample these conformations. Contrastingly, both CP- and OX-DNA sampled conformations with a high roll in the G6G7 base pair step to the same extent in the AGGC sequence context. Furthermore, these differences in roll between CP- and OX-DNA adducts in the TGGA sequence context appear to be preserved in the complexes with HMGB1a.

5.1.2. Overall bend angle

HMGB1a, whose differential binding affinity to CP- and OX-DNA has been experimentally characterized (Malina, et al., 2007; Pil and Lippard, 1992), binds specifically to bent or distorted DNA and bends it further (Bianchi, et al., 1989; Pil, et al., 1993). The formation of the Pt-GG adduct induces a sharp bend in the DNA towards the major groove and results in the formation of a wide and shallow minor groove which provides multiple sites for interaction with HMGB1a (Ohndorf, et al., 1999). The higher bend angle of the Pt-DNA adduct has been postulated to make the binding of HMGB1a to Pt-DNA energetically more favorable compared to undamaged DNA (Pil, et al., 1993), and hence the distribution of the bend angles could influence the preferential binding of HMG-domain proteins to Pt-DNA.

We first examined the propensity of free Pt-DNA to bend. We calculated the overall bend angle of the central 10 base pairs of the different hydrogen-bonded conformations using the program MADBEND (Strahs and Sclick, 2000). The overall distribution of bend angles indicated that the platinated DNA is more bent than undamaged DNA as expected (Figure 5.4). When we compared CP- and OX-GG adducts in the TGGA sequence context, we observed a higher population of structures in CP-GG adduct compared to OX-GG adduct having bend angles close to 58.9º, which is the bend angle of CP-DNA bound to HMGB1a found in its crystal structure (Ohndorf, et al., 1999) (represented as a dashed vertical line in Figure 5.4). When we computed the percentage of species having bend angles ±10º of the bend angle of CP-DNA bound to HMGB1a, we found that CP-GG had 10.25% of the population in this region, while OX-GG adduct had only 5.86% of its population in this region. The situation was reversed in the AGGC sequence context, where OX had 22.15% of the population within ±10º of the bend angle of CP-DNA bound to HMGB1a (in its crystal structure (Ohndorf,

et al., 1999)), while CP-GG adduct had only 15.24% of the population in the higher bend angle region of the distribution.

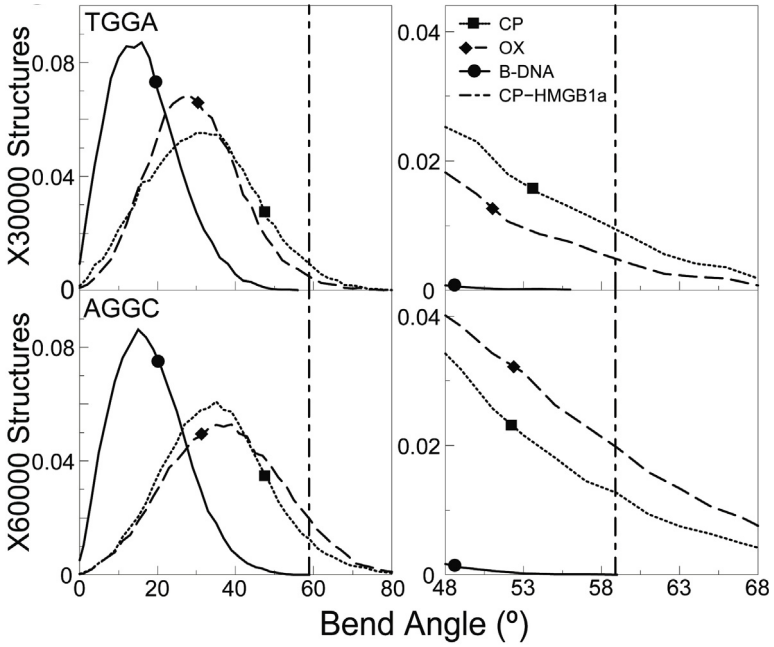

Figure 5.4. Bend angle distributions of CP-, OX- and undamaged DNA
The bend angle distributions of CP-, OX-GG adducts and undamaged DNA in the TGGA and the AGGC sequence context are plotted. The bend angle of DNA in the crystal structure of CP-DNA bound to HMGB1a(Ohndorf, et al., 1999) is plotted as a vertical dashed line. The region of bend angle ±10º of the bend angle in the crystal structure of CP-DNA bound to HMGB1a is plotted alongside to highlight differences between CP- and OX-GG adducts. Reproduced from Srinivas Ramachandran, Brenda R. Temple, Stephen G. Chaney and Nikolay V. Dokholyan, Structural basis for the sequence-dependent effects of platinum-DNA adducts. *Nucleic Acids Research* (2009) 37(8):2434-2448, with permission from Oxford University Press.

Upon clustering the distribution of bend angles based on hydrogen bond formation, we observed significant correlation between hydrogen bond pattern and bend angle (Figure 5.5). In the TGGA sequence context, the A8-N7 hydrogen bond formed by the CP-GG adduct was associated with higher bend angles (mean bend angle of 44.3º) compared to species with no hydrogen bonds (29.8º) and with the G7-O6 hydrogen bond (29.9º). For the OX-GG adduct, no single species stood out with higher mean bend angle. In the AGGC sequence context, the formation of A5-N7 hydrogen bond was associated with a higher bend angle compared to the structures with the G7-O6 hydrogen bond or no hydrogen bonds with the drug for both CP- and OX-GG adducts. In

summary, higher bend angles were associated with hydrogen bond formation to adjacent adenines in both TGGA and AGGC sequence contexts, which gave a significant advantage to the CP-GG adduct in the TGGA sequence context and a slight advantage to the OX-GG adduct in the AGGC sequence context in terms of interaction with HMGB1a.

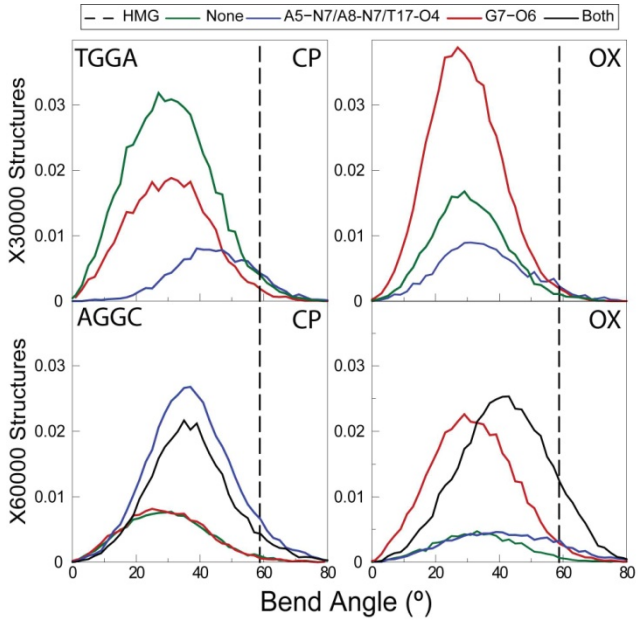

Figure 5.5. Bend Angle distributions of hydrogen-bonded species in the TGGA and AGGC sequence contexts.
The bend angle distributions of different hydrogen-bonded species in CP-TGGA, OX-TGGA, CP-AGGC and OX-AGGC are plotted. The frequency distribution for a particular hydrogen bonded species was obtained from structures that formed that particular hydrogen bond. However, the normalization was performed over the total number of structures (30,000 structures for Pt-DNA in the TGGA sequence context and 60,000 structures for Pt-DNA in the AGGC sequence context) to show the relative abundance of different hydrogen bonded species. The bend angle of DNA in the crystal structure of HMGB1a bound to CP-DNA is shown as a dashed vertical dashed line.

To examine if the behavior of free Pt-DNA in terms of the bend angle was predictive of the HMGB1a-Pt-DNA complex, we analyzed the bend angles calculated from the HMGB1a-Pt-DNA simulations in the three sequence contexts (Figure 5.6). We observe little difference in bend angles of CP- and OX-DNA in the TGGA sequence context, with distribution of CP-DNA having slightly higher values at higher bend angles. In the HMGB1a-Pt-DNA complex, this subtle difference in the bend angle distribution

may not translate to much better binding. However, in TGGT and AGGC sequence context, we observe that the distribution of bend angles of CP-DNA is slightly right-shifted compared to OX-DNA, which may indicate better binding by CP-DNA in these sequences.

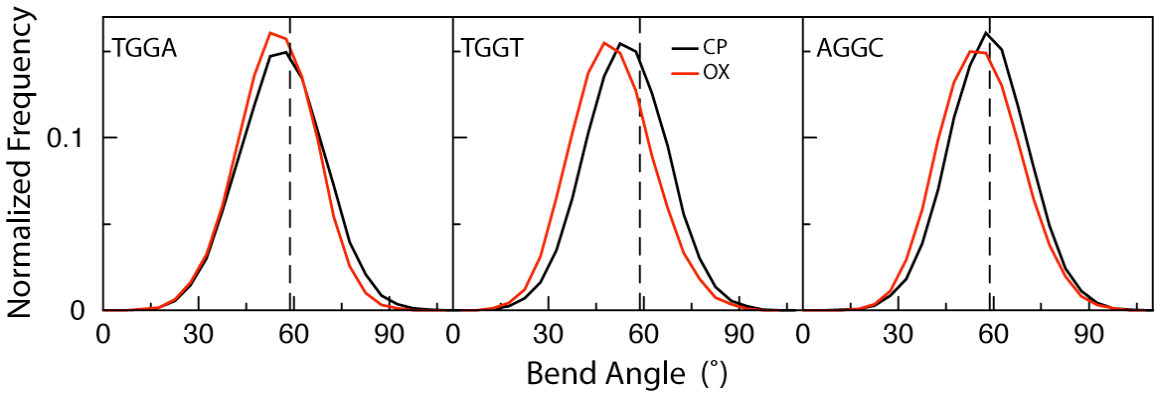

Figure 5.6. Bend angle distributions of CP-, OX-DNA bound to HMGB1a
The bend angle distributions of CP-, OX-GG adducts and undamaged DNA in the TGGA and the AGGC sequence context are plotted. The distribution for undamaged DNA is plotted as a solid line; the distribution for CP-DNA is plotted as a dotted line and that for OX-DNA is plotted as a dashed line. The bend angle of DNA in the crystal structure of CP-DNA bound to HMGB1a (Ohndorf, et al., 1999) is plotted as a vertical dashed line.

5.1.3. Conformations favoring Ser41 Hydrogen bond

In the crystal structure of the HMGB1a-CP-DNA complex in the TGGA sequence context, Ser41 of HMGB1a forms a hydrogen bond with N3 atom of the adenine 3' to Pt-GG adduct(Ohndorf, et al., 1999) (which would correspond to A8 in our simulations of free Pt-DNA). Mutagenesis experiments suggest that this hydrogen bond has a minor (~4-fold) effect on the affinity of HMGB1a for CP-DNA(He, et al., 2000). In our HMGB1a-Pt-DNA simulations, surprisingly, we observe hydrogen bond between S41 and the base 3' to the Pt-GG adduct regardless of the identity of the 3' base or the Pt-drug (Table 5.1). When we calculated the energetic contribution of this hydrogen bond seen in our MD simulations using an orientation dependant hydrogen bonding potential(Ding and Dokholyan, 2006), we observe the mean hydrogen-bond energy due to the Ser41-A hydrogen bond in the CP-HMGB1a complex is 0.78 kcal/mol ± 0.003 (S.E.M), which

compares well with 0.832 kcal/mol observed experimentally (S41A mutation causes four-fold increase in binding dissociation constant) (Table 5.1, Figure 5.7). OX-HMGB1a features the same hydrogen bond of similar energy. However, the TGGT and AGGC sequence contexts feature pyrimidines in the 3' side of the adduct, and hence a SP2 hybridized oxygen (O2). We observe these oxygens to form hydrogen bonds with S41 in our simulations and further, they are almost twice more stabilizing compared to the TGGA sequence context (Table 5.1, Figure 5.7). Thus, we observe S41 forming sequence specific hydrogen bonds with Pt-DNA.

Table 5.1. Summary of hydrogen bond formation between Ser41 and the base 5' to the Pt-GG adduct

Sequence Context	Hydrogen Bonding Atom	Drug	% Occupancy	Mean Hydrogen Bond Energy (kcal/mol)
AGGC	C-O2	CP	89	1.44
		OX	83	1.40
TGGT	T-O2	CP	63	0.99
		OX	80	1.28
TGGA	A-N3	CP	70	0.79
		OX	79	0.87

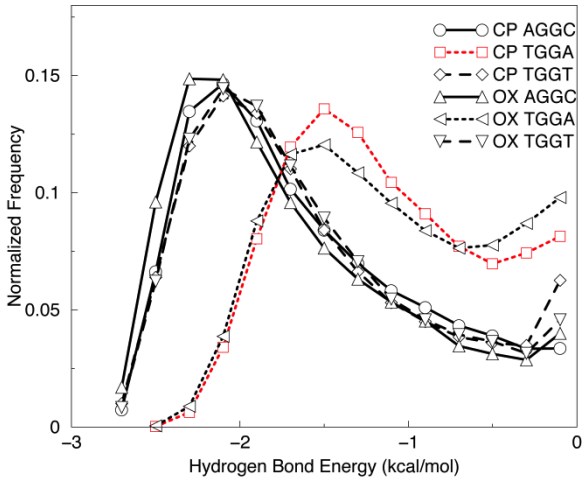

Figure 5.7. Distribution of the strength of hydrogen bond between Ser41 and the base 3' to Pt-GG adduct.
The hydrogen bond strength (energy) was calculated using an orientation dependent hydrogen bond potential for CP- and OX-DNA in TGGA, AGGC and TGGT sequence contexts.

In the HMGB1a-Pt-DNA complexes (in TGGA sequence context), the structures forming the Ser41-A8 hydrogen bond have a G7-A8 slide and twist that is intermediate between that observed in the minor conformations of the free CP- and OX-DNA ensembles. However, the HMGB1a-Pt-DNA conformers containing the Ser41-A8 hydrogen bond have a G7-A8 roll of 0-7.5º and a G7-A8 shift of -1 to 0 Å, which is very close to the conformation of the G7-A8 base-pair step seen in structures with T17-O4 hydrogen bond in free Pt-DNA simulations (Figure 5.8).

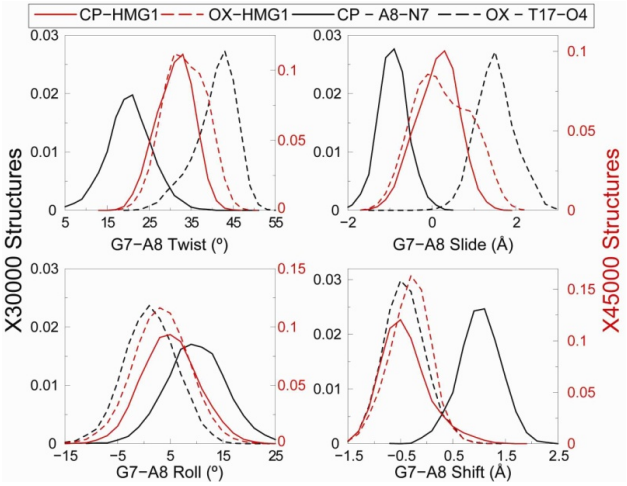

Figure 5.8. Comparison of G7-A8 base-pair step parameters between free and protein bound Pt-DNA in the TGGA sequence context.
Twist, slide, roll and shift parameters of the G7-A8 base-pair step are plotted for structures with CP-A8-N7 hydrogen bond, OX-T17-O4 hydrogen bond, CP- HMGB1a-Ser41-A8-N3 and OX-HMGB1a-Ser41-A8-N3 hydrogen bond. The frequency distribution for a particular hydrogen bonded species was obtained from structures that formed that particular hydrogen bond. However, the normalization was performed over the total number of structures (30,000 structures for free Pt-DNA and 45,000 for HMGB1a bound Pt-DNA) to show the relative abundance of different hydrogen bonded species. To enable comparison of free and bound Pt-DNA (which differ in sampling by an order of magnitude) in the same graph, we employ two Y-axes, which are color-coded. Reproduced from Srinivas Ramachandran, Brenda R. Temple, Stephen G. Chaney and Nikolay V. Dokholyan, Structural basis for the sequence-dependent effects of platinum-DNA adducts. *Nucleic Acids Research* (2009) 37(8):2434-2448, with permission from Oxford University Press.

Thus, structures with the OX-T17-O4 hydrogen bond in free Pt-DNA would aid the formation of Ser41 hydrogen bond during complex formation, while structures with CP-A8-N7 hydrogen bonds have the A8 in a position unfavorable for hydrogen bonding with Ser41 during binding to HMGB1a. The Ser41 occupancy in CP- and OX-DNA in the TGGA sequence context indeed support this prediction from free Pt-DNA; the Ser41

hydrogen bond is observed 79% of the time in complex with OX-DNA compared to 70% in the complex with CP-DNA, resulting in the Ser41 hydrogen bond in the complex with OX-DNA being stronger than in complex with CP-DNA on average(0.87 kcal/mol compared to 0.79 kcal/mol).

5.2. The HMGB1a-Pt-DNA interface

We next analyze the differences in protein-DNA interface between HMGB1a-CP- and HMGB1a-OX-DNA in the TGGA sequence context, where the largest difference in binding affinity is observed experimentally. It is important to note that, in these comparisons, the only difference lies in the carrier-ligand of the drug, which is not even a part of the protein-DNA interface. We use two complementary measures to analyze the interface. The first is the total number of contacts across the protein-DNA interface. We define a contact as any two non-hydrogen atoms being within a distance of 5 Å. Since our force fields are pairwise additive, the number of contacts would be a reliable predictor of the strength of the overall core/interface. Secondly, we analyze contacts between individual protein residue and DNA base. These comparisons also rely on the number of contacts between the residue and the base, but provide information at a resolution higher than that of total number of interface contacts. Furthermore, the number of contacts between individual residue and base points to regions in the interface that feature the differences between the two systems being compared.

5.2.1. CP-DNA forms more interface contacts compared to OX-DNA

We first analyzed the distribution of total number of interface contacts formed by CP- and OX-DNA in complex with HMGB1a. We observed that the distribution of total number of interface contacts in OX-DNA fitted well to a single Gaussian distribution centered at 705 ± 77. CP-DNA fitted well to two Gaussian distributions centered at 741±75 and 836±57 (Figure 5.9). Thus, the distribution of number of interface contacts

observed in CP-DNA is significantly right-shifted compared to OX-DNA. Furthermore, the second Gaussian distribution representing CP-DNA features much more contacts than the first distribution, which is around the same range as OX-DNA. The higher number of contacts in CP-DNA would indicate a stronger complex of HMGB1a with CP-DNA compared to OX-DNA as seen experimentally.

To analyze this phenomenon further, we divided the CP-DNA ensemble into two extreme regions (shown shaded in Figure 5.9): the “high contacts” structures that form the right half of the second Gaussian distribution, and the “low contacts” structures that form the left half of the first Gaussian distribution. Utilizing only the extreme halves of the Gaussian distributions ensures that we do not analyze features of the interface that might be common to these two distributions, thereby leading to inconsistent conclusions.

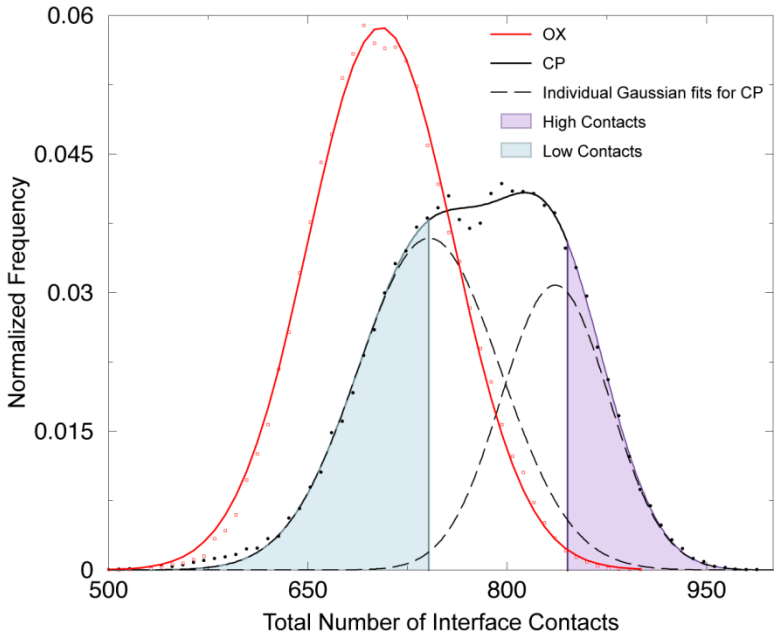

Figure 5.9. Distribution of the total number of interface contacts seen in HMGB1a complex with CP-DNA and OX-DNA
Black dots and red squares represent the raw distribution for CP- and OX-DNA respectively. The solid lines are the fitted Gaussian distributions. The dashed lines represent the individual Gaussian distributions that are added up to fit to the distribution of CP-DNA. The shaded regions represent the high and low contact ensembles.

5.2.2 Pt-GG roll correlates with number of interface contacts

We asked if the higher number of interface contacts in CP-DNA compared to OX-DNA was due to increased flexibility of CP-DNA as evidenced by the roll of the Pt-GG base-pair step. To test this hypothesis, we divided the distribution of the Pt-GG roll into quartiles and constructed a distribution of the number of Protein-DNA interface contacts corresponding to structures in each of the quartiles of the Pt-GG roll distributions. We observe that for both CP- and OX-DNA, the mean number of interface contacts increases as we proceed from the structures in the lowest to the highest quartile of the Pt-GG roll. Of course, this effect is much more pronounced in CP-DNA due to the presence of much higher number of interface contacts when compared to OX-DNA (Figure 5.10).

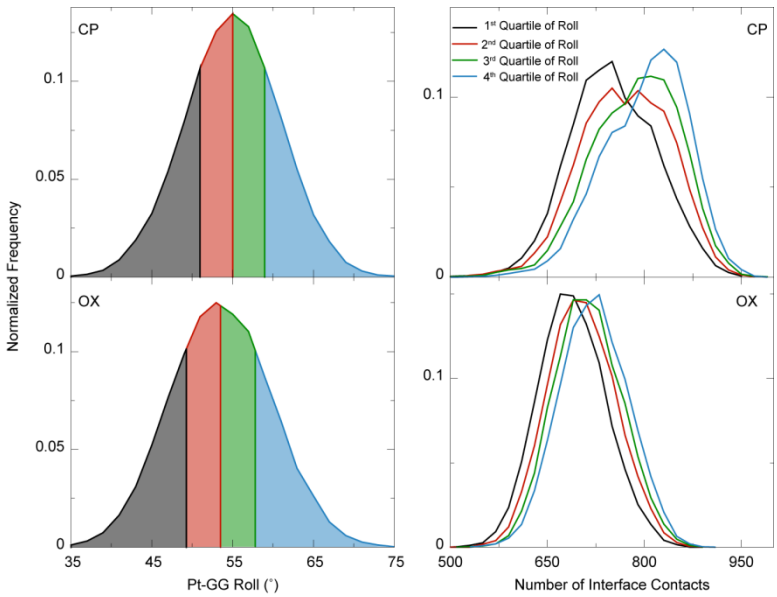

Figure 5.10. Distribution of the number of interface contacts of structures that are part of different quartiles of the Pt-GG roll distribution.
The division of the Pt-GG distribution is illustrated in the left panel, with structures corresponding to each quartile shaded in black, red, green and blue respectively. The distribution of total interface contacts of the structures corresponding to each of these quartiles is plotted in the right panel in the respective colors. We can observe the distributions shifting to the right as we move from the first quartile to the fourth.

When we look at the reverse question, i.e., does the high-contact ensemble feature much higher roll than the low-contact ensemble, we find that indeed the

difference between the Pt-GG roll of OX-DNA and high-contact ensemble is much higher the difference seen in comparing CP-DNA overall and OX-DNA(Figure 5.11). More importantly, the low-contact ensemble has a distribution of Pt-GG roll identical to OX-DNA. Thus, one of the physical basis of higher roll leading to higher affinity would be the better formation of protein-DNA interface at higher roll angles of the Pt-GG base-pair step.

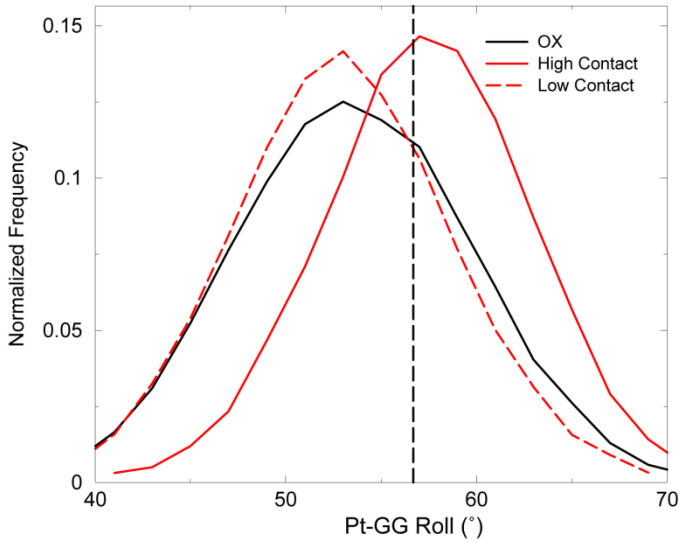

Figure 5.11. The distribution of Pt-GG roll of OX-DNA and different ensembles of CP-DNA bound to HMGB1a.
The Pt-GG roll of high-contact and low-contact ensemble of CP-DNA and the overall distribution for OX-DNA are plotted.

5.2.3 Comparison of protein-DNA interface between CP- and OX-DNA

The difference in number of interface contacts between CP- and OX-DNA could arise due to two scenarios. In the first scenario, CP-DNA could be forming some distinct contacts with HMGB1a that are not seen in OX-DNA complex. In the second scenario, same residues in HMGB1a may be forming contacts in both CP- and OX-DNA, but in CP-DNA, these residues may pack better against DNA, leading to a higher number of contacts. The two scenarios lead to different ways to control the differential binding affinity of HMGB1a to CP- and OX-DNA. In the first scenario, mutating the residues forming contacts only with CP-DNA could abrogate differential affinity. In the second

scenario, it is the flexibility of Pt-DNA as a whole that is contributing to a better interface with HMGB1a overall.

In order to understand the origin of the difference in number of interface contacts between CP- and OX-DNA, we analyzed the contact map of the protein-DNA interface. The contact map plots out the number of atomic contact between each residue of the protein and each base of the DNA in the form of a matrix (the protein residues are on the X-axis and the DNA bases on the Y-axis). By comparing the contact map calculated from the crystal structure with those obtained from OX-DNA and CP high- and low-contact ensembles, we observe that the contacts seen in the crystal structure are well preserved in both CP- and OX-DNA (Figure 5.12).

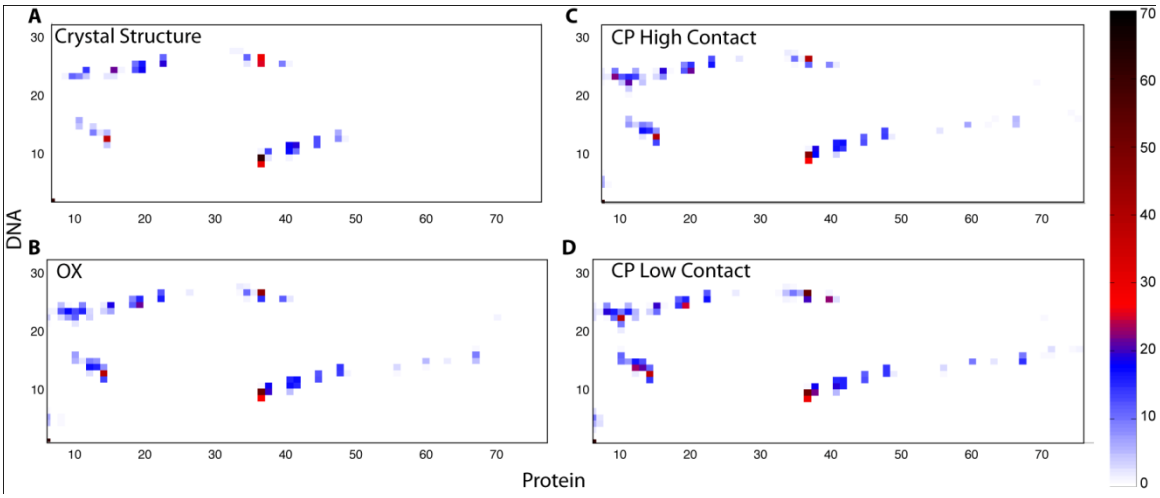

Figure 5.12. Contact maps of the HMGB1a-Pt-DNA interface
Each square on the contact map represents the interaction between a protein residue and a DNA base. The color of the square indicates the number of heavy atom contacts involving the residue and the base. The scale of color used is shown on right. The contact maps are plotted for the crystal structure (A), the overall OX-DNA ensemble (B), the high contact ensemble (C) and low contact ensemble (D) of CP-DNA.

We also observe additional contacts in CP- and OX-DNA corresponding to the N-terminal and C-terminal tails that do not adopt any secondary structure. In the crystal structure, these regions are static, thus forming fewer contacts compared to the MD ensembles, where they form much more contacts. Comparing CP- and OX-DNA reveals that they too form similar contacts. Thus, the observed difference in the total number of

interface contacts should arise from the differences in the strength of the same contacts formed by CP- and OX-DNA. To explore this idea further, we next plot the difference contact map. Here, the contact map of OX-DNA is subtracted from the maps of overall CP-DNA, high contact and low contact (Figure 5.13).

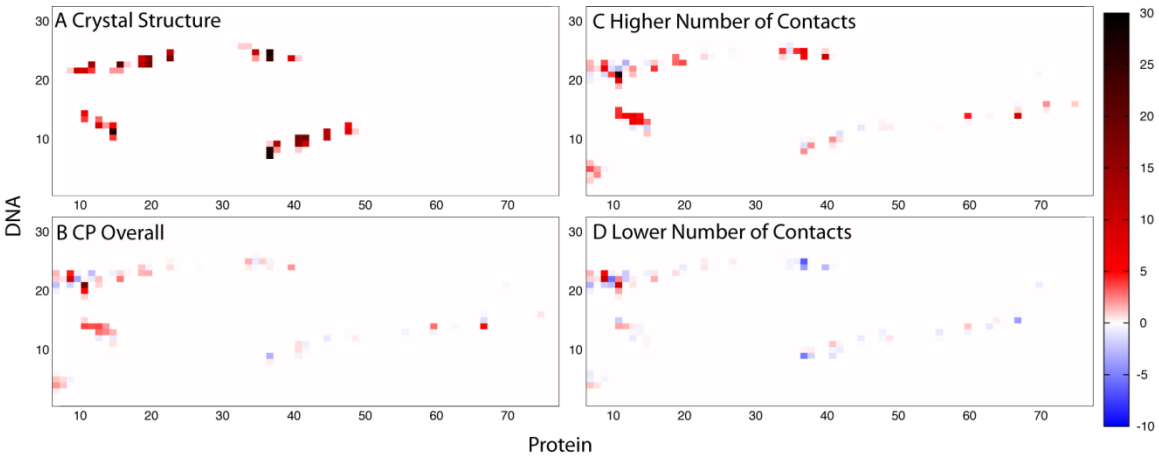

Figure 5.13. Difference Contact maps of the HMGB1a-Pt-DNA interface
The difference contact map obtained by subtracting the OX-DNA contact map from the overall CP-DNA contact map (B), the contact map of high contact ensemble (C) and the contact map of the low contact ensemble (D) are shown. The contact map of the crystal structure (A) is plotted for reference. The scale of differences (from -10 to 30) is shown on right.

In this difference map, blue colors would indicate more contacts formed in OX-DNA between a residue and a base, while red and black colors would indicate stronger contacts formed by CP-DNA. Even when comparing overall CP- and OX-DNA, we find several contacts are stronger in CP-DNA compared to OX-DNA. This effect is even more pronounced in the high contact ensemble, while several places, especially Phe37 show more favorable contacts with OX-DNA when compared with the low contact ensemble. In order to explore if there is a specific region in the interface that shows up preferentially in high contact ensemble when compared with OX-DNA, we highlighted all the protein residues that form at least 3 more contacts on average with high contact ensemble compared to OX-DNA (Figure 5.14). As expected from the difference map, we observe residues right from the 5'side of the adduct to the end of DNA on the interface having a difference in number of contacts between OX-DNA and the high contact ensemble. In

summary, we find that CP-DNA has a higher number of interface contacts compared to OX-DNA mainly due to the fact that the interface as a whole forms more contacts rather than distinct residues in CP- and OX-DNA forming differential contacts.

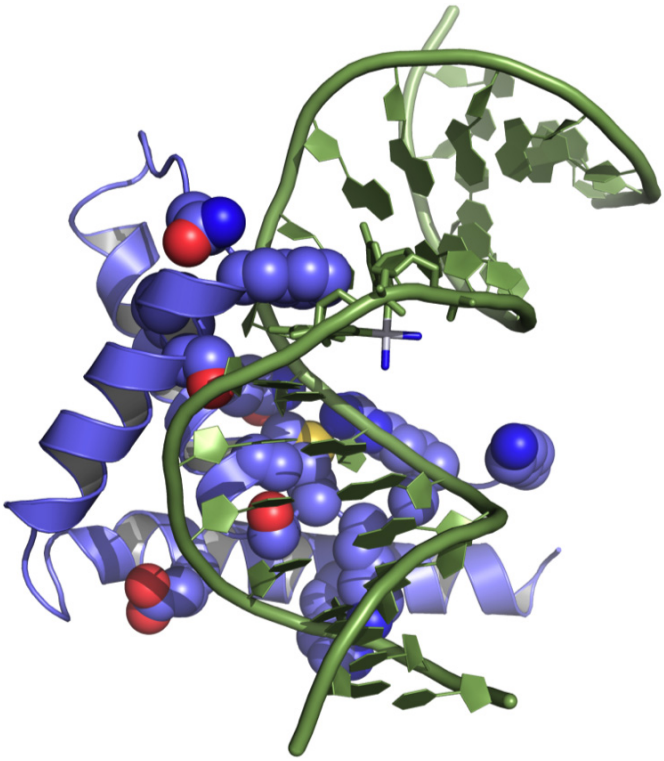

Figure 5.14. The HMGB1a-CP-DNA complex showing residues that formed increased number of contacts with CP-DNA compared to OX-DNA.
The protein and DNA molecules are shown in cartoon representation, with the residues that form at least 3 contacts more in high-contact CP-DNA ensemble compared to OX-DNA are shown as scaled spheres. The figure was created using PyMOL (www.pymol.org)

5.3. Conclusions

We analyzed the free and bound Pt-DNA ensembles for structural characteristics that report on their ability to bind HMGB1a. Based on the structural data available for HMGB1a, we can summarize the main parameters that influence binding as the roll of the Pt-GG base-pair step, the overall bend angle, the Ser41 hydrogen bond. The analysis of free Pt-DNA ensembles provided insight into the discriminating factors in the recognition step of complex formation, while analysis of the HMGB1a-Pt-DNA ensembles provided insight on the final tight complex of protein and DNA. Regarding

Phe37 intercalation, in free Pt-DNA, we found that CP-DNA had a higher population of structures in the region of Pt-GG roll that was favorable for Phe37 intercalation compared to OX-DNA. Thus, in terms of recognition by Phe37, CP-DNA was in a more favorable conformation for larger amount of time compared to OX-DNA. Similarly when HMGB1a was bound, CP-DNA displayed higher mean Pt-GG roll, implying better intercalation by Phe37 compared to OX-DNA.

With respect to the Ser41 hydrogen bond, the free Pt-DNA simulations revealed that clearly, OX-DNA was poised to form this interaction much better than CP-DNA. The conformation on the 3' side of the minor conformations of free OX-DNA was favorable for the formation of the Ser41 hydrogen bond. Similarly, in the bound form, OX-DNA formed this hydrogen bond ~10% more compared to CP-DNA, mainly because of CP-DNA's preference to form the A8-N7 hydrogen bond, which placed the 3' base in a conformation that was unfavorable for the formation of Ser41 hydrogen bond. Interestingly, we observe similar hydrogen bonds by Ser41 in all three sequence contexts we studied, indicating the adaptability of HMGB1a to various sequences. The energetic contribution of the Ser41 hydrogen bond however is much higher in AGGC and TGGT sequence contexts compare to the TGGA sequence context.

Finally, the interface of HMGB1a with the minor groove of Pt-DNA plays an important role in determining the overall binding affinity of HMGB1a to Pt-DNA. Strikingly, we observe CP-DNA to form more interface contacts in the minor groove compared to OX-DNA. Thus, clearly CP-DNA will feature higher binding affinity to HMGB1a compared to OX-DNA according to our simulations, which is what is observed experimentally also. Unexpectedly, we found that Pt-GG roll also correlated with the strength of the rest of the binding interface. Higher roll was accompanied by higher number of interface contacts. This observation lead us to conclude that the Pt-GG roll

and hence the flexibility of Pt-DNA is responsible for the extent of interface formed by HMGB1a. Furthermore, by analyzing the interface contact map, we determined that the effect of forming higher number of contacts arises from contributions from all regions of the interface and not just few distinctive contacts. Thus, the interface analysis shows that higher flexibility of Pt-DNA results in an overall tighter complex with HMGB1a.

Chapter 6. Conclusions and Future Directions

6.1. Conclusions

We started this study with the hypothesis that the differences in binding affinities of different proteins to CP- and OX-DNA could arise due to the differences in flexibility that are seldom observed in an average conformation. Our main hypothesis arose due to the fact that many experimental structures of CP- and OX-DNA did not yield significant differences, which in the face of differential binding affinities in the molecular level and differential efficacies at the cellular level posed an intriguing challenge. We proposed to use molecular dynamics simulations, which can efficiently probe the short time-scale dynamics of small biomolecular systems in the vicinity of their native states, to uncover the differences in flexibility between CP- and OX-DNA adducts. In Chapter 3, we described the results of the first such simulations on free Pt-DNA. We discovered not surprisingly, that the major conformations of CP- and OX-DNA are very similar. These data agreed well with the experimental structural studies, since the structural studies obtain the major conformation most efficiently. However, we discovered significant differences in regimes invisible to experimental studies. Only the latest techniques are able to probe the minor conformations of biomolecules experimentally (Ref. (Iwahara, et al., 2004) for example), and these studies have been restricted to a few model systems. Thus, MD simulations provide the best alternative to probe minor conformations that are close to native state. We found that the minor conformations of CP- and OX-DNA in the TGGA sequence context have distinct conformations on the 3' side of the adduct. TGGA is the sequence in which HMGB1a exhibits the highest differential binding affinity

towards CP- and OX-DNA. Furthermore, HMGB1a binds asymmetrically to Pt-DNA, with most interactions on the 3' side of the adduct. Thus, simulations of free Pt-DNA by themselves provided important clues towards the origin of the differential binding affinity through differences in flexibility, and the presence of minor conformations. The carrier ligand dependent differences in conformation seen in TGGA sequence context was analyzed more comprehensively by considering TGGT and AGGC sequence contexts in Chapter 4. These analyses sought to characterize all possible carrier ligand and sequence context dependent conformational states in a systematic manner.

Each of the predictions from free Pt-DNA was tested using the simulations of HMGB1a-Pt-DNA in Chapter 5. We found that the predictions for roll of the platinated base-pair step and for the formation of Ser41 hydrogen bond were confirmed during the analysis of the protein-Pt-DNA ensemble. Interestingly, we also discovered the propensity of Ser41 to form hydrogen bonds with the base 3' of Pt-GG adduct regardless of its identity. These hydrogen bonds demonstrate the ability of HMGB1a to form interactions even with the base (as opposed to DNA backbone) in a sequence independent manner. The importance of Pt-GG roll beyond intercalation by Phe37 was revealed by the positive correlation between the roll and the number of interface contacts. We also observed that the increased number of contacts seen in CP-DNA compared to OX-DNA was due to an overall increase in strength of contacts rather than a few distinctive contacts that were seen in CP-DNA but not in OX-DNA. This result combined with the correlation between roll and number of contacts strongly indicates that the main basis for differential binding affinity of HMGB1a to CP- and OX-DNA is due to the differences in flexibility of CP- and OX-DNA adducts. The difference in flexibility is most prominent in the TGGA and AGGC sequence contexts, but due to binding of

HMGB1a through the 3' side of the adduct, this difference translates to differential binding affinity of HMGB1a significantly in the TGGA sequence context.

6.2. Future Directions

Our identified mechanism of differential binding could be applicable to a wide range of proteins that need not even possess an HMG-domain. Many of the proteins that are known to bind Pt-DNA adducts recognize distorted DNA and/or bind through the minor groove. In terms of both mode of recognition (distorted DNA) and mode of binding (minor groove), flexibility of Pt-DNA will play a major role in determining binding affinity. After our explicit demonstration of the effect of difference in flexibility translated into differences in the strength of the binding interface in HMGb1a, we can use a similar approach to rationalize differential binding by other proteins. One of the proteins that has been shown to have differential binding affinity to CP- and OX-DNA is tata binding protein (TBP) (Vichi, et al., 1997). TBP binds through the minor groove and has specific residues that intercalate DNA (Juo, et al., 1996). It will be interesting to study HMG-domain proteins like SRY and LEF-1 because they bind DNA in a symmetric manner as opposed to HMGB1a that binds on the 3' side of the adduct. Further structural studies of Pt-DNA binding to TBP, LEF-1 and SRY among other proteins will confirm our hypothesis regarding flexibility of Pt-DNA and binding affinity.

Our studies have also highlighted how a carrier ligand could influence a Pt-drug's biological effect. Our main motivation to perform this study was to answer the question: Given that CP- and OX-DNA form similar adducts on similar sites of DNA, what could be the basis of their differential efficacies. The 53 fold difference in binding affinity to HMGB1a itself could have profound impact on drug sensitivity by different tumors. Studies at the cellular level, tracking the effect of HMGB1a on sensitivity to CP and OX will inform us if the large difference in binding affinity of HMGB1a to CP- and OX-DNA is

responsible for the differential efficacy. Such studies have been difficult in the past because of the large degeneracy in HMG-domain proteins in the cell. However, current RNAi techniques can help in broad suppression of all HMG-domain containing genes for short periods to discern the effect of these proteins on cellular sensitivity to CP and OX.

Our systematic analysis of the interface between HMGB1a and minor groove of Pt-DNA has shown several residues to have differential contacts with CP- and OX-DNA. Future studies can study the impact of mutating these residues identified in our study on the differential binding affinity of CP- and OX-DNA. Furthermore, we were able to discern through our simulations the differential strength of Ser41 hydrogen bonds in different sequence contexts and in CP- and OX-DNA. Thus, the Ser41Ala mutation in HMGB1a will have differential effects on binding affinity that is dependent upon both the sequence context and the carrier ligand. Hence, binding experiments with Ser41Ala HMGB1a will yield new insights on sequence specificity of HMGB1a with respect to Pt-DNA.

To conclude, our simulations of free Pt-DNA and HMGB1a-Pt-DNA helped explain the effect of sequence context and carrier ligand on HMGB1a binding affinity to Pt-DNA. Furthermore, our studies have led to several predictions that can be tested experimentally in the future.

Bibliography

Aebi, S., Kurdihaidar, B., Gordon, R., Cenni, B., Zheng, H., Fink, D., Christen, R.D., Boland, C.R., Koi, M., Fishel, R. and Howell, S.B. (1996) Loss of DNA mismatch repair in acquired resistance to cisplatin, *Cancer Res.*, **56**, 3087-3090.

Baik, M.H., Friesner, R.A. and Lippard, S.J. (2003) Theoretical study of cisplatin binding to purine bases: why does cisplatin prefer guanine over adenine?, *J.Am.Chem Soc.*, **125**, 14082-14092.

Bancroft, D.P., Lepre, C.A. and Lippard, S.J. (1990) 195Pt NMR kinetic and mechanistic studies of cis- and trans-diamminedichloroplatinum(II) binding to DNA, *J.Am.Chem.Soc.*, **112**, 6860-6871.

Bassett, E., King, N.M., Bryant, M.F., Hector, S., Pendyala, L., Chaney, S.G. and Cordeiro-Stone, M. (2004) The role of DNA polymerase h in translesion synthesis past platinum-DNA adducts in human fibroblasts, *Cancer Res.*, **64**, 6469-6475.

Bassett, E., Vaisman, A., Havener, J.M., Masutani, C., Hanaoka, F. and Chaney, S.G. (2003) Efficiency of extension of mismatched primer termini across from cisplatin and oxaliplatin adducts by human DNA polymerases beta and eta in vitro, *Biochemistry*, **42**, 14197-14206.

Bellacosa, A. (2001) Functional interactions and signaling properties of mammalian DNA mismatch repair proteins, *Cell Death Differ*, **8**, 1076-1092.

Bianchi, M.E., Beltrame, M. and Paonessa, G. (1989) Specific recognition of cruciform DNA by nuclear protein HMG1, *Science*, **243**, 1056-1059.

Binks, S.P. and Dobrota, M. (1990) Kinetics and mechanism of uptake of platinum based pharmaceuticals by the rat small intestine, *Biochemical Pharmacology*, **40**, 1329-1336.

Bosl, G.J., Bajorin, D.F., Sheinfeld, J., Motzer, R.J. and Chaganti, R.S.K. (2008) Cancer of the testis. In DeVita, V.T., Lawrence, T.S. and Rosenberg, S.A. (eds), *Cancer: principles & practice of oncology*. Lippincott Williams and Wilkins, Philadelphia, PA, 1463.

Brown, S.J., Kellett, P.J. and Lippard, S.J. (1993) Ixr1, a yeast protein that binds to platinated DNA and confers sensitivity to cisplatin, *Science*, **261**, 603-605.

Chaney, S.G., Campbell, S.L., Bassett, E. and Wu, Y. (2005) Recognition and processing of cisplatin- and oxaliplatin-DNA adducts, *Crit Rev Oncol Hematol*, **53**, L3-11.

Chaney, S.G. and Vaisman, A. (1999) Specificity of platinum-DNA adduct repair, *J Inorg Biochem*, **77**, 71-81.

Chow, C.S., Whitehead, J.P. and Lippard, S.J. (1994) HMG domain proteins induce sharp bends in cisplatin-modified DNA, *Biochemistry*, **33**, 15124-15130.

Chvalova, K., Sari, M.A., Bombard, S. and Kozelka, J. (2008) LEF-1 recognition of platinated GG sequences within double-stranded DNA. Influence of flanking bases, *J Inorg Biochem*, **102**, 242-250.

Ciarimboli, G., Ludwig, T., Lang, D., Pavenstadt, H., Koepsell, H., Piechota, H.J., Haier, J., Jaehde, U., Zisowsky, J. and Schlatter, E. (2005) Cisplatin nephrotoxicity is critically mediated via the human organic cation transporter 2, *Am.J.Pathol.*, **167**, 1477-1484.

Cornell, W.D., Cieplak, P., Bayly, C.I., Gould, I.R., Merz, K.M., Ferguson, D.M., Spellmeyer, D.C., Fox, T., Caldwell, J.W. and Kollman, P.A. (1995) A Second Generation Force Field for the Simulation of Proteins, Nucleic Acids, and Organic Molecules, *Journal of the American Chemical Society*, **117**, 5179-5197.

Ding, F. and Dokholyan, N.V. (2006) Emergence of protein fold families through rational design, *PLoS Comput Biol*, **2**, e85.

Drummond, J.T., Anthoney, A., Brown, R. and Modrich, P. (1996) Cisplatin and adriamycin resistance are associated with MutL alpha and mismatch repair deficiency in an ovarian tumor cell line, *The Journal of Biological Chemistry*, **271**, 19645-19648.

Duan, Y., Wu, C., Chowdhury, S., Lee, M.C., Xiong, G., Zhang, W., Yang, R., Cieplak, P., Luo, R., Lee, T., Caldwell, J., Wang, J. and Kollman, P. (2003) A point-charge force field for molecular mechanics simulations of proteins based on condensed-phase quantum mechanical calculations, *J Comput Chem*, **24**, 1999-2012.

Eastman, A. (1987) The formation, isolation and characterization of DNA adducts produced by anticancer platinum complexes, *Pharmacol Ther*, **34**, 155-166.

Fink, D., Nebel, S., Aebi, S., Zheng, H., Cenni, B., Nehme, A., Christen, R.D. and Howell, S.B. (1996) The role of mismatch repair in platinum drug resistance, *Cancer Res.*, **56**, 4881-4886.

Furuta, T., Ueda, T., Aune, G., Sarasin, A., Kraemer, K.H. and Pommier, Y. (2002) Transcription-coupled nucleotide excision repair as a determinant of cisplatin sensitivity of human cells, *Cancer Res.*, **62**, 4899-4902.

Gale, G.R., Morris, C.R., Atkins, L.M. and Smith, A.B. (1973) Binding of an antitumor platinum compound to cells as influenced by physical factors and pharmacologically active agents, *Cancer Res.*, **33**, 813-818.

Gately, D.P. and Howell, S.B. (1993) Cellular accumulation of the anticancer agent cisplatin - A review, *Br.J.Cancer*, **67**, 1171-1176.

Gelasco, A. and Lippard, S.J. (1998) NMR solution structure of a DNA dodecamer duplex containing a cis-diammineplatinum(II) dGpG intrastrand cross-link, the major adduct of the anticancer drug cisplatin, *Biochemistry*, **37**, 9230-9239.

Havener, J.M., McElhinny, S.A., Bassett, E., Gauger, M., Ramsden, D.A. and Chaney, S.G. (2003) Translesion synthesis past platinum DNA adducts by human DNA polymerase mu, *Biochemistry*, **42**, 1777-1788.

Havener, J.M., Nick McElhinny, S.A., Bassett, E., Gauger, M., Ramsden, D.A. and Chaney, S.G. (2003) Translesion Synthesis Past Platinum DNA Adducts by Human DNA Polymerase μ, *Biochemistry*, **42**, 1777-1788.

He, Q., Ohndorf, U.M. and Lippard, S.J. (2000) Intercalating residues determine the mode of HMG1 domains a and B binding to cisplatin-modified DNA, *Biochemistry*, **39**, 14426-14435.

Herman, F., Kozelka, J., Stoven, V., Guittet, E., Girault, J.P., Huynh-Dinh, T., Igolen, J., Lallemand, J.Y. and Chottard, J.C. (1990) A d(GpG)-platinated decanucleotide duplex is kinked An extended NMR and molecular mechanics study, *European Journal of Biochemistry*, **194**, 119-133.

Hromas, R.A., North, J.A. and Burns, C.P. (1987) Decreased cisplatin uptake by resistant L1210 leukemia cells, *Cancer Lett.*, **36**, 197-201.

Huang, J.C., Zamble, D.B., Reardon, J.T., Lippard, S.J. and Sancar, A. (1994) HMG-domain proteins specifically inhibit the repair of the major DNA adduct of the anticancer drug cisplatin by human excision nuclease, *Proc Natl Acad Sci U S A*, **91**, 10394-10398.

Iwahara, J., Schwieters, C.D. and Clore, G.M. (2004) Characterization of nonspecific protein-DNA interactions by 1H paramagnetic relaxation enhancement, *J Am Chem Soc*, **126**, 12800-12808.

Jiricny, J. (2006) The multifaceted mismatch-repair system, *Nat Rev Mol Cell Biol*, **7**, 335-346.

Jung, Y. and Lippard, S.J. (2003) Nature of Full-Length HMGB1 Binding to Cisplatin-Modified DNA, *Biochemistry*, **42**, 2664-2671.

Jung, Y. and Lippard, S.J. (2007) Direct Cellular Responses to Platinum-Induced DNA Damage, *Chemical Reviews*, **107**, 1387-1407.

Juo, Z.S., Chiu, T.K., Leiberman, P.M., Baikalov, I., Berk, A.J. and Dickerson, R.E. (1996) How proteins recognize the TATA box, *J Mol Biol*, **261**, 239-254.

Lavery, R. and Sklenar, H. (1996) Curves 5.1: Helical Analysis of Irregular Nucleic Acids. *Institut de Biologie PhysicoChimique*.

Lawrence, D.L., Engelsberg, B.N., Farid, R.S., Hughes, E.N. and Billings, P.C. (1993) Localization of the binding region of high mobility group protein 2 to cisplatin-damaged DNA, *J Biol Chem*, **268**, 23940-23945.

Love, J.J., Li, X., Case, D.A., Giese, K., Grosschedl, R. and Wright, P.E. (1995) Structural basis for DNA bending by the architectural transcription factor LEF-1, *Nature*, **376**, 791-795.

Malina, J., Novakova, O., Vojtiskova, M., Natile, G. and Brabec, V. (2007) Conformation of DNA GG intrastrand cross-link of antitumor oxaliplatin and its enantiomeric analog, *Biophysical Journal*, **93**, 3950-3962.

Marzilli, L.G., Saad, J.S., Kuklenyik, Z., Keating, K.A. and Xu, Y. (2001) Relationship of solution and protein-bound structures of DNA duplexes with the major intrastrand cross-link lesions formed on cisplatin binding to DNA, *J.Am.Chem.Soc.*, **123**, 2764-2770.

McA'Nulty, M.M. and Lippard, S.J. (1996) The HMG-domain protein Ixr1 blocks excision repair of cisplatin-DNA adducts in yeast, *Mutation Research/DNA Repair*, **362**, 75-86.

McAnulty, M.M. and Lippard, S.J. (1996) The HMG-domain protein Ixr1 blocks excision repair of cisplatin- DNA adducts in yeast, *Mutat.Res-DNA.Repair*, **362**, 75-86.

Ohndorf, U.-M., Rould, M.A., He, Q., Pabo, C.O. and Lippard, S.J. (1999) Basis for recognition of cisplatin-modified DNA by high-mobility-group proteins, *Nature*, **399**, 708-712.

Ohndorf, U.M., Whitehead, J.P., Raju, N.L. and Lippard, S.J. (1997) Binding of tsHMG, a mouse testis-specific HMG-domain protein, to cisplatin-DNA adducts, *Biochemistry*, **36**, 14807-14815.

Page, J.D., Husain, I., Sancar, A. and Chaney, S.G. (1990) Effect of the diaminocyclohexane carrier ligand on platinum adduct formation, repair, and lethality, *Biochemistry*, **29**, 1016-1024.

Pil, P.M., Chow, C.S. and Lippard, S.J. (1993) High-Mobility-Group-1 Protein Mediates DNA Bending as Determined by Ring Closures, *Proceedings of the National Academy of Sciemces of the United States of America*, **90**, 9465-9469.

Pil, P.M. and Lippard, S.J. (1992) Specific binding of chromosomal protein HMG1 to DNA damaged by the anticancer drug cisplatin, *Science*, **256**, 234-237.

Pinto, A.L. and Lippard, S.J. (1985) Binding of the antitumor drug cis-diamminedichloroplatinum(II) (cisplatin) to DNA, *Biochim.Biophys.Acta*, **780**, 167-180.

Press, W.H., Flannery, B.P., Teukolsky, S.A. and Vetterling, W.T. (1992) *Numerical Recipes in C: The Art of Scientific Computing* Cambridge University Press, Cambridge.

Raymond, E., Faivre, S., Woynarowski, J.M. and Chaney, S.G. (1998) Oxaliplatin-mechanism of action and antineoplastic activity, *Seminars.in Oncology*, **25**, 4-12.

Reardon, J.T., Vaisman, A., Chaney, S.G. and Sancar, A. (1999) Efficient nucleotide excision repair of cisplatin, oxaliplatin, and bis-aceto-amine-dichloro-cyclohexylamine-platinum(IV) (JM216) platinum intrastrand DNA diadducts, *Cancer Res.*, **59**, 3968-3971.

Rixe, O., Ortuzar, W., Alvarez, M., Parker, R., Reed, E., Paull, K. and Fojo, T. (1996) Oxaliplatin, tetraplatin, cisplatin, and carboplatin: Spectrum of activity in drug-resistant cell lines and in the cell lines of the National Cancer Institute's Anticancer Drug Screen panel, *Biochemical Pharmacology*, **52**, 1855-1865.

Safaei, R. and Howell, S.B. (2005) Copper transporters regulate the cellular pharmacology and sensitivity to Pt drugs, *Crit Rev Oncol Hematol*, **53**, 13-23.

Scheeff, E.D., Briggs, J.M. and Howell, S.B. (1999) Molecular modeling of the intrastrand guanine-guanine DNA adducts produced by cisplatin and oxaliplatin, *Molecular Pharmacology*, **56**, 633-643.

Schmidt, W. and Chaney, S.G. (1993) Role of carrier ligand in platinum resistance of human carcinoma cell lines, *Cancer Res.*, **53**, 799-805.

Sharma, S., Gong, P., Temple, B., Bhattacharyya, D., Dokholyan, N.V. and Chaney, S.G. (2007) Molecular dynamic simulations of cisplatin- and oxaliplatin-d(GG) intrastand cross-links reveal differences in their conformational dynamics, *J Mol Biol*, **373**, 1123-1140.

Siddik, Z.H. (2003) Cisplatin: mode of cytotoxic action and molecular basis of resistance, *Oncogene*, **22**, 7265-7279.

Spingler, B., Whittington, D.A. and Lippard, S.J. (2001) 2.4 A crystal structure of an oxaliplatin 1,2-d(GpG) intrastrand cross-link in a DNA dodecamer duplex, *Inorg Chem*, **40**, 5596-5602.

Strahs, D. and Sclick, T. (2000) A-Tract Bending: Insights into Experimental Structures by Computational Models, *Journal of Molecular Biology*, **301**, 643-663.

Svejstrup, J.Q. (2003) Rescue of arrested RNA polymerase II complexes, *J Cell Sci*, **116**, 447-451.

Takahara, P.M., Frederick, C.A. and Lippard, S.J. (1996) Crystal structure of the anticancer drug cisplatin bound to duplex DNA, *J.Am.Chem.Soc.*, **118**, 12309-12321.

Treiber, D.K., Zhai, X., Jantzen, H.M. and Essigmann, J.M. (1994) Cisplatin-DNA adducts are molecular decoys for the ribosomal RNA transcription factor hUBF (human upstream binding factor), *Proc Natl Acad Sci U S A*, **91**, 5672-5676.

Vaisman, A., Lim, S.E., Patrick, S.M., Copeland, W.C., Hinkle, D.C., Turchi, J.J. and Chaney, S.G. (1999) Effect of DNA polymerases and high mobility group protein 1 on the carrier ligand specificity for translesion synthesis past platinum-DNA adducts, *Biochemistry*, **38**, 11026-11039.

Vaisman, A., Masutani, C., Hanaoka, F. and Chaney, S.G. (2000) Efficient translesion replication past oxaliplatin and cisplatin GpG adducts by human DNA polymerase eta, *Biochemistry*, **39**, 4575-4580.

Vaisman, A., Varchenko, M., Umar, A., Kunkel, T.A., Risinger, J.I., Barrett, J.C., Hamilton, T.C. and Chaney, S.G. (1998) The role of hMLH1, hMSH3, and hMSH6

defects in cisplatin and oxaliplatin resistance: correlation with replicative bypass of platinum-DNA adducts, *Cancer Res*, **58**, 3579-3585.

Vichi, P., Coin, F., Renaud, J.P., Vermeulen, W., Hoeijmakers, J.H.J., Moras, D. and Egly, J.M. (1997) Cisplatin- and UV-damaged DNA lure the basal transcription factor TFIID/TBP, *The EMBO Journal*, **16**, 7444-7456.

Volp, K., Brezniceanu, M.-L., Bosser, S., Brabletz, T., Kirchner, T., Gottel, D., Joos, S. and Zornig, M. (2006) Increased expression of high mobility group box 1 (HMGB1) is associated with an elevated level of the antiapoptotic c-IAP2 protein in human colon carcinomas, *Gut*, **55**, 234-242.

Wang, D. and Lippard, S.J. (2005) Cellular processing of platinum anticancer drugs, *Nat.Rev.Drug Discov.*, **4**, 307-320.

Weaver, D.A., Crawford, E.L., Warner, K.A., Elkhairi, F., Khuder, S.A. and Willey, J.C. (2005) ABCC5, ERCC2, XPA and XRCC1 transcript abundance levels correlate with cisplatin chemoresistance in non-small cell lung cancer cell lines, *Mol.Cancer*, **4**, 18.

Webb, M., Payet, D., Lee, K.B., Travers, A.A. and Thomas, J.O. (2001) Structural requirements for cooperative binding of HMG1 to DNA minicircles, *J Mol Biol*, **309**, 79-88.

Wei, M., Cohen, S.M., Silverman, A.P. and Lippard, S.J. (2001) Effects of spectator ligands on the specific recognition of intrastrand platinum-DNA cross-links by high mobility group box and TATA-binding proteins, *J Biol Chem*, **276**, 38774-38780.

Weiss, R.B. and Christian, M.C. (1993) New Cisplatin Analogues in Development - A Review, *Drugs*, **46**, 360-377.

Werner, M.H., Huth, J.R., Gronenborn, A.M. and Clore, G.M. (1995) Molecular basis of human 46X,Y sex reversal revealed from the three- dimensional solution structure of the human SRY-DNA complex, *Cell*, **81**, 705-714.

Wu, H.I., Brown, J.A., Dorie, M.J., Lazzeroni, L. and Brown, J.M. (2004) Genome-wide identification of genes conferring resistance to the anticancer agents cisplatin, oxaliplatin, and mitomycin C, *Cancer Res.*, **64**, 3940-3948.

Wu, Y., Bhattacharyya, D., King, C.L., Baskerville-Abraham, I., Huh, S.H., Boysen, G., Swenberg, J.A., Temple, B., Campbell, S.L. and Chaney, S.G. (2007) Solution structures of a DNA dodecamer duplex with and without a cisplatin 1,2-d(GG) intrastrand cross-link: Comparison with the same DNA duplex containing an oxaliplatin 1,2-d(GG) intrastrand cross-link, *Biochemistry*, **46**, 6477-6487.

Wu, Y., Pradhan, P., Havener, J., Boysen, G., Swenberg, J.A., Campbell, S.L. and Chaney, S.G. (2004) NMR solution structure of an oxaliplatin 1,2-d(GG) intrastrand cross-link in a DNA dodecamer duplex, *J Mol Biol*, **341**, 1251-1269.

Yang, D., van Bloom, S.S.G.E., Reedijk, J., van Bloom, J.H. and Wang, A.H.J. (1995) Structure and isomerization of an intrastrand cisplatin-cross-linked octamer DNA duplex by NMR analysis, *Biochemistry*, **34**, 12912-12920.

Yao, S., Plastaras, J.P. and Marzilli, L.G. (1994) A molecular mechanics AMBER-type force field for modeling platinum complexes of guanine derivatives, *Inorganic Chemistry*, **33**, 6061-6077.

Yarnell, A.T., Oh, S., Reinberg, D. and Lippard, S.J. (2001) Interaction of FACT, SSRP1, and the high mobility group (HMG) domain of SSRP1 with DNA damaged by the anticancer drug cisplatin, *The Journal of Biological Chemistry*, **276**, 25736-25741.

Yonezawa, A., Masuda, S., Yokoo, S., Katsura, T. and Inui, K.I. (2006) Cisplatin and oxaliplatin, but not carboplatin and nedaplatin, are substrates for human organic cation transporters (SLC22A1-3 and multidrug and toxin extrusion family), *J.Pharmacol.Exp.Ther.*, **319**, 879-886.

Zamble, D.B., Mu, D., Reardon, J.T., Sancar, A. and Lippard, S.J. (1996) Excision repair studies of cisplatin-DNA adducts, *Biochemistry*, **35**, 10004-10013.

Zhai, X., Beckmann, H., Jantzen, H.M. and Essigmann, J.M. (1998) Cisplatin-DNA adducts inhibit ribosomal RNA synthesis by hijacking the transcription factor human upstream binding factor, *Biochemistry*, **37**, 16307-16315.